Center for Modeling of Turbulence and Transition
Research Briefs - 1991

Runge-Kutta Methods Combined with Compact Difference Schemes for the Unsteady Euler Equations

Sheng-Tao Yu

1. Motivation and Objective

Recent development using compact difference schemes to solve the Navier-Stokes equations show spectral-like accuracy[1,2]. In this paper, we report further study of the numerical characteristics of various combinations of the Runge-Kutta (RK) methods and compact difference schemes to calculate the unsteady Euler equations. Conventionally, the accuracy of finite difference schemes is assessed based on the evaluations of dissipative error. The objectives are reducing the numerical damping and, at the same time, preserving numerical stability. While this approach has tremendous success solving steady flows, numerical characteristics of unsteady calculations remain largely unclear. For unsteady flows, in addition to the dissipative errors, phase velocity and harmonic content of the numerical results are of concern. As a result of the discretization procedure, the simulated unsteady flow motions actually propagate in a dispersive numerical medium. Consequently, the dispersion characteristics of the numerical schemes which relate the phase velocity and wave number may greatly impact the numerical accuracy. The objective of the present paper is to assess the numerical accuracy of the simulated results. To this end, the Fourier analysis is performed to provide the dispersive correlations of various numerical schemes.

First, a detailed investigation of the existing RK methods is carried out. A generalized form of an N-step RK method is derived. With this generalized form, the criteria are derived for the three and four-step RK methods to be third and fourth-order time accurate for the non-linear equations, e.g., flow equations. These criteria are then applied to commonly used RK methods such as Jameson's 3-step and 4-step[3,4] schemes and Wray's algorithm[5] to identify the accuracy of the methods. For the spatial discretization, compact difference schemes are presented. The schemes are formulated in the operator-type[6] to render themselves suitable for the Fourier analyses. The results of the analyses provide CFL limits, the numerical dispersion relations, and the artificial damping required for stable and time-accurate solutions.

Finally, the performance of the numerical methods is demonstrated by numerical examples. The first case is a quasi-one-dimensional calculation of the acoustic admittance in a converging nozzle. The CFD results are compared with Tsien's analytical solution[7]; the harmonic content of this flow field is limited to one frequency mode. All numerical schemes of concern provide accurate solutions. The second case is a one-dimensional simulation of a shocked sound wave. The harmonic

content is complex and distinct differences between various schemes are observed. The results are also compared with the analytical solution provided by Morse and Ingard[8]. In the one-dimensional cases, details of the numerical methods in setting up the initial conditions and the perturbation on the computational boundary are described.

The third case is a two-dimensional simulation of a Lamb vortex[9] in an uniform flow. This calculation provides a realistic assessment of various finite difference schemes in terms of the conservation of the vortex strength and the harmonic content after travelling a substantial distance. The numerical implementation of Giles' non-reflective equations[17] coupled with the characteristic equations as the boundary condition is discussed in detail. Finally, the single vortex calculation is extended to simulate vortex pairing[10]. For the distance between two vortices less than a threshold value, numerical results show crisp resolution of the vortex merging.

2. Work Accomplished

2.1 Numerical Method

The Euler equations in Cartesian coordinates can be cast into a vector form:

$$\frac{\partial \mathbf{Q}}{\partial t} + \sum_{i=1}^{3} \frac{\partial \mathbf{E}_i}{\partial x_i} = 0, \tag{1}$$

where $\mathbf{Q}$ is the unknown vector and $\mathbf{E}_i$ is the inviscid flux in the x_i direction. The Runge-Kutta algorithm is applied as the temporal discretization and the second, fourth, and sixth-order compact difference schemes are applied to the spatial discretization.

2.2.1 The Runge-Kutta Method

The use of the Runge-Kutta methods for flow equations stems from the application of the methods to solve ordinary differential equations (ODEs). An ODE has one independent variable and its solution is obtained by integrating the equation from its initial condition. When one applies the Runge-Kutta method to the flow equations, time is treated as the independent variable as is in an ODE, and the convective terms are taken as the inhomogeneous part of the equations, such as

$$\frac{\partial Q}{\partial t} = R(Q). \tag{2}$$

Notice that the boldface symbols which represent vectors have been temporarily dropped for typographic convenience. In addition, all results in the following discussion are valid for both scalar and vector equations.

The Runge-Kutta methods have algorithms of the form

$$Q^{n+1} = Q^n + \Delta t \hat{R}(Q^n, \Delta t), \tag{3}$$

where the increment function $\hat{R}(Q^n, \Delta t)$ is a suitable chosen approximation to the inhomogeneous part of the equation, that is, $R(Q)$. In general, the calculation of the increment function $\hat{R}$ is subdivided into N steps on the interval $t^n \leq t \leq t^{n+1}$. And the final increment function $\hat{R}$ is a weighted average of the inhomogeneous terms evaluated at the different steps on the interval $t^n \leq t \leq t^{n+1}$, that is

$$\begin{aligned} Q^1 &= Q^n + \Delta t(\alpha_{11} R^n), \\ Q^2 &= Q^n + \Delta t(\alpha_{21} R^n + \alpha_{22} R^1), \\ Q^3 &= Q^n + \Delta t(\alpha_{31} R^n + \alpha_{32} R^1 + \alpha_{33} R^2), \\ &\vdots \\ Q^{n+1} &= Q^n + \Delta t(\alpha_{N1} R^n + \alpha_{N2} R^1 + \cdots + \alpha_{NN} R^{N-1}), \end{aligned} \tag{4}$$

where the superscript $n, 1, 2, \ldots,$ and $n+1$ denote the time steps on the time interval $t^n \leq t_1 \leq t_2 \leq \ldots \leq t_N \leq t^{n+1}$, and α_{ij} is the weighting factor for the step i and term j. There are $\sum_{i=1}^{N} i$ weighting coefficients to be determined and an infinite number of coefficient sets can be chosen. However, certain criteria must be met for the algorithm to retain high-order accuracy.

In what follows, the criteria of the coefficient set of a 3-step Runge-Kutta method to be third-order accurate is given. To proceed, we follow the conventional approach and expand all inhomogeneous terms R^i in Eqn. (4) to a Taylor's series about R^n and drop all terms in which the exponent of Δt is greater than 3. The result is compared with its analytical counterpart by equating terms in like powers of Δt. The result is tabulated in Table 1. For the convenience of the discussion, the following simplification of symbols is activated: R denotes $R(Q^n)$, Q denotes Q^n, R' denotes $(\partial R/\partial Q)^n$, and R'' denotes $(\partial^2 R/\partial Q^2)^n$. In addition to the equality of the coefficients of all the powers of Δt, we also want the equality of the coefficients of the functions of R, R', and R''. As a result, we find the criteria of the coefficients for the 3-step RK methods to be third-order accurate as,

$$\alpha_{31} + \alpha_{32} + \alpha_{33} = 1, \tag{5a}$$

$$\alpha_{11}\alpha_{32} + \alpha_{33}(\alpha_{21} + \alpha_{22}) = \frac{1}{2}, \tag{5b}$$

$$\alpha_{11}^2\alpha_{32} + (\alpha_{21} + \alpha_{22})^2\alpha_{33} = \frac{1}{3}, \tag{5c}$$

$$\alpha_{11}\alpha_{22}\alpha_{33} = \frac{1}{6}. \tag{5d}$$

Equations (5a) and (5b) are the criteria of first and second order accuracy, respectively. The remaining equations are of third order term. Since four equations contain six unknowns, the system is underdetermined, and two of the coefficients may be chosen arbitrarily. The obvious choice is to let the two coefficients be null to reduce intermediate storage and numerical operations. According to Eqn. (5d),

none of α_{ii} where $i = 1, 2, 3$, could be zero, and one can set the two of the three remaining coefficients to be zero. Therefore, at least one of the intermediate steps has two non-zero coefficients. Consequently, one needs to store two steps of intermediate solutions for the 3-step, third-order RK methods.

A 3-step Runge-Kutta method proposed by Jameson et al.[3] to solve flow equations is

$$\begin{aligned} Q^1 &= Q^n + \Delta t R^n, \\ Q^2 &= Q^n + \frac{\Delta t}{2}(R^n + R^1), \\ Q^{n+1} &= Q^n + \frac{\Delta t}{2}(R^n + R^2). \end{aligned} \tag{6}$$

It can be shown that the weighting coefficients of the 3-step method satisfy only Eqns. (5a) and (5b). And the method is second-order accurate in time.

Wray[5] proposed another 3-step method,

$$\begin{aligned} Q^1 &= Q^n + \Delta t(\frac{8}{15}R^n), \\ Q^2 &= Q^1 + \Delta t(\frac{5}{12}R^n - \frac{17}{60}R^1), \\ Q^{n+1} &= Q^2 + \Delta t(\frac{3}{4}R^n - \frac{5}{12}R^2). \end{aligned} \tag{7}$$

This formula may be manipulated to fit the generalized form as proposed in Eqn. (4), and we obtain,

$$\begin{aligned} Q^1 &= Q^n + \Delta t(\frac{8}{15}R^n), \\ Q^2 &= Q^n + \Delta t(\frac{1}{4}R^n + \frac{5}{12}R^1), \\ Q^{n+1} &= Q^n + \Delta t(\frac{1}{4}R^n + \frac{3}{4}R^2). \end{aligned} \tag{8}$$

Wray's coefficients match all the equations in Eqn. (5) and therefore the scheme is third-order accurate. In this formula, α_{32} is set to zero and two sets of solutions are needed in the second and the third steps. The calculation can be carried out by either the vectorized algorithm proposed by Wray, or straightforward calculation according to Eqns. (7) and (8).

A similar procedure can be applied to the 4-step Runge-Kutta methods, and the criteria for the scheme to be fourth-order accurate are:

$$\alpha_{41} + \alpha_{42} + \alpha_{43} + \alpha_{44} = 1, \tag{9a}$$

$$\alpha_{11}\alpha_{42} + (\alpha_{21} + \alpha_{22})\alpha_{43} + (\alpha_{31} + \alpha_{32} + \alpha_{33})\alpha_{44} = \frac{1}{2}, \tag{9b}$$

$$\alpha_{11}^2\alpha_{42} + (\alpha_{21}+\alpha_{22})^2\alpha_{43} + (\alpha_{31}+\alpha_{32}+\alpha_{33})^2\alpha_{44} = \frac{1}{3}, \tag{9c}$$

$$\alpha_{11}\alpha_{22}\alpha_{43} + [\alpha_{11}\alpha_{32} + (\alpha_{21}+\alpha_{22})\alpha_{33}]\,\alpha_{44} = \frac{1}{6}, \tag{9d}$$

$$\alpha_{11}^3\alpha_{42} + (\alpha_{21}+\alpha_{22})^3\alpha_{43} + (\alpha_{31}+\alpha_{32}+\alpha_{33})^3\alpha_{44} = \frac{1}{4}, \tag{9e}$$

$$\begin{aligned} &\frac{1}{2}\alpha_{11}^2\alpha_{22}\alpha_{43} + (\alpha_{21}+\alpha_{22})\alpha_{11}\alpha_{22}\alpha_{43} \\ &+\frac{1}{2}\left[(\alpha_{21}+\alpha_{22})^2\alpha_{33} + \alpha_{11}^2\alpha_{32}\right]\alpha_{44} \\ &+(\alpha_{31}+\alpha_{32}+\alpha_{33})\left[\alpha_{11}\alpha_{32} + (\alpha_{21}+\alpha_{22})\alpha_{33}\right]\alpha_{44} = \frac{1}{6}, \end{aligned} \tag{9f}$$

$$\alpha_{11}\alpha_{22}\alpha_{33}\alpha_{44} = \frac{1}{24}. \tag{9g}$$

Equations (9a) and (9b) are for first and second-order accuracy, respectively. Equations (9c) and (9d) are for third-order accuracy. The remaining equations are for the fourth-order terms. Here, seven equations contain ten unknowns, and three of the coefficients may be chosen arbitrarily.

A 4-step RK method attributed to Kutta[11] for solving ODEs was adopted by Jameson et al.[3] to solve the flow equations. The algorithm can be expressed as,

$$\begin{aligned} Q^1 &= Q^n + \frac{\Delta t}{2}R^n, \\ Q^2 &= Q^n + \frac{\Delta t}{2}R^1, \\ Q^3 &= Q^n + \Delta t R^2, \\ Q^{n+1} &= Q^n + \frac{\Delta t}{6}(R^n + 2R^1 + 2R^2 + R^3). \end{aligned} \tag{10}$$

The coefficients satisfy Eqn. (9) and the algorithm is fourth-order accurate. However, this method requires all four intermediate solutions in the final step. As a result, the use of this scheme for large-scale calculations is undesirable.

Later on, Jameson and Baker[4] proposed another 4-step algorithm,

$$\begin{aligned} Q^1 &= Q^n + \frac{\Delta t}{4}R^n, \\ Q^2 &= Q^n + \frac{\Delta t}{3}R^1, \\ Q^3 &= Q^n + \frac{\Delta t}{2}R^2, \\ Q^{n+1} &= Q^n + \Delta t R^3. \end{aligned} \tag{11}$$

This scheme was proposed to calculate the steady state solutions and the transient solutions were not of concern. For that purpose, the algorithm is convenient to

program and no intermediate solution needs to be stored. For the present investigation, however, the weighting coefficients of this method satisfy only part of Eqn. (9) and the algorithm is second-order accurate. Nevertheless, this formulation is favorable compared to a 2-step, second-order RK method because part of the third and fourth-order terms are satisfied, namely, Eqns. (9d) and (9g). Consequently, a larger marching step, i.e., a larger CFL number, could be used.

2.2.2 Compact Difference Schemes

The remaining task of discretizing the flow equations is the spatial differencing of the inviscid fluxes. An effective manner for generating a high-order, central difference scheme is the compact difference method. The scheme is obtained by using only three and five points to achieve fourth-order and sixth-order accuracy in space, respectively. The gain in the accuracy is not based on the involvement of more points as in the conventional approach, but on implicitly solving the derivatives simultaneously at all locations. According to Hermite's generalization of a Taylor's series,[12] one can get

$$u'_{i-1} + 4u'_i + u'_{i+1} = \frac{3}{\Delta x}(u_{i+1} - u_{i-1}) + O(\Delta x^4), \tag{12}$$

$$u'_{i-1} + 3u'_i + u'_{i+1} = \frac{1}{12\Delta x}(u_{i+2} + 28u_{i+1} - 28u_{i-1} - u_{i-2}) + O(\Delta x^6), \tag{13}$$

where the superscript $'$ represents the spatial derivatives. Equation (12) is the fourth-order method and Eqn. (13) is the sixth-order one. When the fourth-order method is used in the interior nodes, a third-order biased implicit scheme[13] is adopted for grid nodes at the computational boundary, such as

$$\begin{aligned} 2u'_1 + 4u'_2 &= \frac{1}{\Delta x}(-5u_1 + 4u_2 + u_3) + O(\Delta x^3), \\ 2u'_{max} + 4u'_{max-1} &= \frac{1}{\Delta x}(5u_{max} - 4u_{max-1} - u_{max-2}) + O(\Delta x^3). \end{aligned} \tag{14}$$

When the sixth-order method is used in the interior nodes, the fourth-order scheme, Eqn. (12), is used at locations one grid node away from the boundary and the third-order biased scheme is used at the boundary. The application of the implicit compact difference schemes with the appropriate boundary conditions involves the inversion of a scalar tridiagonal matrix. The inversion of the matrix incurs little penalty in terms of CPU time.

2.3 Fourier Analysis

By definition, any function, $u(x,t)$, which is continuous, periodic, and square summable can be expressed in a Fourier series expansion at a constant time,

$$u(x,t) = \sum_{k=-\infty}^{\infty} \hat{u}(k,t) e^{i2\pi kx/L} \tag{15}$$

where L is the period of the function $u(x,t)$, k is the wave number, and i is $\sqrt{-1}$. The Fourier coefficient is defined as,

$$\hat{u}(k,t) = \frac{1}{L}\int_{-L/2}^{L/2} u(x,t)e^{-i2\pi kx/L}dx. \tag{16}$$

In the Fourier analysis of a finite difference scheme, functions are defined at discrete points. The discrete Fourier series and its coefficients are defined analogous to their continuous counterparts,

$$\begin{aligned} u_j^n &= \sum_{k=0}^{K-1} \hat{u}^n(k)e^{i2\pi kj/K}, \quad j = 0, \pm 1, \pm 2, \cdots, \pm\infty, \\ \hat{u}^n(k) &= \frac{1}{K}\sum_{j=1}^{K} u_j^n e^{-i2\pi kj/K}, \quad k = 0, 1, \cdots, K-1. \end{aligned} \tag{17}$$

Here, the length of the computational domain L is decomposed into K grid nodes ($L = K\Delta x$). The superscript n denotes the time step and the subscript j is the spatial location index. Similar to the continuous function, the algebraic system in terms of the function $exp(i2\pi kj/K)$ is periodic over the computational domain L (or K) and orthonormal, such as

$$\begin{aligned} e^{i2\pi kj/K} &= e^{i2\pi k(j+K)/K} \\ \frac{1}{K}\sum_{j=0}^{K-1} e^{i2\pi k_1 j/K} e^{-i2\pi k_2 j/K} &= \delta_{k_1 k_2} \end{aligned} \tag{18}$$

where $\delta_{k_1 k_2}$ is the Kronecker delta. Therefore, the establishment of the discrete Fourier series and coefficients is self-sufficient, and is not an approximation of its continuous counterpart.

As shown in Eqns. (17) and (18), the harmonic content of the discretized equation is limited to the number of grid nodes used in the computational domain. A discrete solution u_j^n at a location (j) and time (n) is a linear combination of K wave modes. The Fourier analysis is performed by substituting each wave mode of the discrete Fourier expansion, Eqn. (17), into the discretized flow equations to calculate the amplification factor, $g(k)$, which is defined as

$$g(k) = \frac{\hat{u}^{n+1}(k)}{\hat{u}^n(k)}. \tag{19}$$

The procedure is repeated for all wave modes ($k = 0, 1, \cdots, K-1$) and the full spectrum of the amplification factor is obtained. In this process, we map the function u in terms of spatial variable x on the interval $[-L/2, L/2]$ to the wave number space on $[-\pi, \pi]$ assuming that the analysis is local for an infinite and periodic domain. Therefore, the solution of the amplification factor on the interval $[-\pi, 0]$ is

the complex conjugate of that on $[0, \pi]$. For this reason, the results of our Fourier analyses are presented on the interval $[0, \pi]$.

In the present investigation, one-dimensional equations are considered for the Fourier analysis. In addition, we can perform a similarity transformation to transform the one-dimensional Euler equations to their characteristic form, i.e., three decoupled scalar equations. Consequently, a scalar, advective equation on a periodic domain is adopted as the model equation in our analysis,

$$\frac{\partial u}{\partial t} + \lambda \frac{\partial u}{\partial x} = 0, \tag{20}$$

where the phase velocity (λ) is equivalent to the eigenvalues of the Euler equations, namely $u - c$, $u + c$, and u where u is velocity and c is the speed of sound. The phase speed (λ) is treated as a parameter in the Fourier analysis to avoid the Fourier convolution, therefore the analysis is linear. For the unsteady calculations, the requirement of the time resolution of the flow field restricts the time marching step. In other words, the variations of flow properties between time steps are small. Thus, linear analysis is a viable tool.

In what follows, the procedure to obtain the amplification factor of the model equation discretized by Runge-Kutta methods and compact differences is illustrated. First, the generalized forms of the amplification factor for the 3 and 4-step Runge-Kutta methods are derived. These representations of the amplification factors are independent of the spatial discretization schemes. From the equations of Wray's 3-step scheme, Eqn.(7), we have

$$\begin{aligned} g^1 &= 1 + \frac{8}{15} Z, \\ g^2 &= 1 + \frac{1}{4} Z + \frac{5}{12} Z g^1, \\ g &= 1 + \frac{1}{4} Z + \frac{3}{4} Z g^2, \end{aligned} \tag{21}$$

where

$$\begin{aligned} g^1 Q^n &= Q^1, \\ g^2 Q^n &= Q^2, \\ g Q^n &= Q^{n+1}. \end{aligned} \tag{22}$$

The variable Z represents the spatial discretization applied to the convective term ($-\lambda \partial u / \partial x$). By substituting the amplification factors of the intermediate steps, g^1 and g^2, into the last step of Wray's algorithm, we obtain the amplification factor, g, for the 3-step scheme,

$$g = 1 + Z + \frac{1}{2} Z^2 + \frac{1}{6} Z^3. \tag{23}$$

It is interesting to note that Eqn. (23) can be directly derived from the Taylor's series expansion by adopting the invariance property of the time and spatial derivatives of the model equation, i.e., $Z = -\lambda \partial u/\partial x = \partial u/\partial t$. This is valid because the coefficients satisfy Eqn. (5), which is deduced from the Taylor's series expansion up to the third-order term. On the other hand, the amplification factor of the 3-step scheme proposed by Jameson et al., Eqn. (6), can be derived as

$$g = 1 + Z + \frac{1}{2}Z^2 + \frac{1}{4}Z^3. \tag{24}$$

It is obvious that the scheme is not third-order accurate.

A similar analysis can be applied to the 4-step methods. Identical forms of the amplification factors of both 4-step methods of concern (Eqns. (10) and (11)) are obtained, such as

$$g = 1 + Z + \frac{1}{2}Z^2 + \frac{1}{6}Z^3 + \frac{1}{24}Z^4. \tag{25}$$

Unlike the case of the 3-step schemes, the effect of the order of accuracy of these two 4-step schemes does not appear in the expression of the amplification factor. This is because the amplification factor is derived based on the linearized equation. Only by using Eqns. (5) and (9), which take into account nonlinear terms, can one justify the order of the accuracy of the RK schemes.

The remaining task is to derive the explicit form of the spatial discretization operation, Z, of compact difference schemes. The fourth-order compact difference method, Eqn. (12), can be cast into the operator-type by defining

$$\delta^2 u_i = u_{i+1} - 2u_i + u_{i-1}, \tag{26}$$

where u_i could be any flow property of interest at grid point i. As a result, the fourth-order method can be rewritten as,

$$\left(1 + \frac{\delta^2}{6}\right)\left(\frac{\partial u}{\partial x}\right)_i = \frac{1}{2\Delta x}\left(u_{i+1} - u_{i-1}\right) + O(\Delta x^4). \tag{27}$$

This equation allows us to express $(\partial u/\partial x)_i$ in an explicit form,

$$\left(\frac{\partial u}{\partial x}\right)_x = \left(1 + \frac{\delta^2}{6}\right)^{-1}\left(\frac{u_{i+1} - u_{i-1}}{2\Delta x}\right) + O(\Delta x^4). \tag{28}$$

To proceed, we substitute this explicit, discretized form, Eqn. (32), into the model equation, and we obtain

$$Z^{(4)} = -\frac{6F sin(\hat{k})i}{4 + 2cos(\hat{k})}, \tag{29}$$

where F is the CFL number which is defined as $F = \lambda\Delta t/\Delta x$, and $\hat{k}$ is the normalized wave number ($\hat{k} = 2\pi k/K$) .

It is interesting to note that if the solution reaches a steady state solution, i.e., the time derivative term is zero, the operator $(1 + \delta^2/6)^{-1}$ in the discretized equation becomes futile and the spatial discretization is represented by $(u_{i+1} - u_{i-1})/2\Delta x$, which is only second-order accurate. However, the steady state solution of the one-dimensional wave equation is a constant and the spatial accuracy is meaningless. On the other hand, the accuracy of multi-dimensional calculations is more complex. For example, consider a two-dimensional version of the model equation discretized by the fourth-order compact difference method, and we have

$$\frac{\partial u}{\partial t} + \lambda_x \left(1 + \frac{\delta_x^2}{6}\right)^{-1} \left(\frac{u_{i+1,j} - u_{i-1,j}}{2\Delta x}\right) + \lambda_y \left(1 + \frac{\delta_y^2}{6}\right)^{-1} \left(\frac{u_{i,j+1} - u_{i,j-1}}{2\Delta y}\right) = 0. \tag{30}$$

Again, the operators $(1 + \delta_x^2/6)$ and $(1 + \delta_y^2/6)$ are scalar tridiagonal matrices with the dimensions $IL \times IL$ and $JL \times JL$, respectively. IL and JL are the numbers of the grid nodes in the x and y directions of the computational domain. When $IL = JL$, two operators are identical. We then multiply Eqn. (30) by the operator $(1 + \delta_x^2/6)$ and obtain the steady state equation as

$$\lambda_x \frac{u_{i+1,j} - u_{i-1,j}}{2\Delta x} + \lambda_y \frac{u_{i,j+1} - u_{i,j-1}}{2\Delta y} = 0. \tag{31}$$

Therefore, the steady state solution is only second-order accurate.

Similarly, the spatial discretization of the sixth-order compact difference scheme can be represented in the operator-type such as,

$$\frac{\partial u}{\partial x} = \left(1 + \frac{\delta^2}{5}\right)^{-1} \frac{1}{60\Delta x} (u_{i+2} + 28u_{i+1} - 28u_{i-1} - u_{i-2}) + O(\Delta x^6). \tag{32}$$

And we obtain,

$$Z^{(6)} = -\frac{F[4\sin(\hat{k})\cos(\hat{k}) + 56\sin(\hat{k})]i}{12[2\cos(\hat{k}) + 3]}. \tag{33}$$

Again, when solving the steady state solution with same number of grid nodes in each direction of the computational domain, the spatial discretization is represented by $(u_{i+2} + 28u_{i+1} - 28u_{i-1} - u_{i-2})/60\Delta x$. Unlike the case of the fourth-order scheme, this representation does not match any conventional central difference scheme and it is at most second-order accurate.

According to the above discussion, we can obtain the amplification factor $g(\hat{k})$ for various combinations of the Runge-Kutta methods and compact difference schemes. The amplification factor $g(\hat{k})$ is a complex number and can be expressed as $g(\hat{k}) =$

$exp[i\hat{\omega}(\hat{k})]$, where $\hat{\omega}$ is the normalized frequency and is defined as $\hat{\omega} = 2\pi\omega\Delta t/\tau$, ω is the frequency, τ is the the time period of function u_j^n, and the phase speed (λ) is equal to L/τ. Here, the dissipative and dispersive artifacts of the numerical schemes can be assessed:

1. Dissipation. The normalized frequency $\hat{\omega}$ is a complex number ($\hat{\omega} = \alpha + i\beta$) and its imaginary part represents the magnitude of the amplification factor, i.e.,

$$\begin{aligned} g(\hat{k}) &= e^{i\hat{\omega}} = e^{-\beta}e^{i\alpha} \\ |g(\hat{k})| &= e^{-\beta} \end{aligned} \tag{34}$$

   The magnitude of the amplification factor is the artificial dissipation. When $|g| \geq 1$, the scheme is unstable. For the calculations of unsteady flows, we want $|g|$ to be less than unity but very close to it to ensure numerical stability with minimum artificial dissipation. In the following section, we plot $|g|$ against $\hat{k}$ to illustrate the artificial dissipation.

2. Dispersion. According to Eqn. (34), the relation of $\alpha(\hat{k})$ and $\hat{k}$ represents the artificial dispersion. We plot $\hat{\alpha} = \alpha/F$ against $\hat{k}$ to show phase velocities. Notice that the model equation is dispersionless and the phase velocity is a constant, i.e., λ. After being normalized by the CFL number, the exact solution is a straight line with 45^o angle on the plot of $\hat{\alpha}$ against $\hat{k}$.

Figure 1 shows the results of the Fourier analysis of the third-order Runge-Kutta (RK3) method combined with fourth (CD4), and sixth (CD6) order compact difference schemes and the conventional second-order central difference scheme (CD2). The figures show the dissipative as well as dispersive effects at CFL numbers from 0.4 to 1.4 with an increment of 0.2 between neighboring curves. Figure 1a shows the dissipation of the RK3-CD6 scheme. The method is unstable for CFL numbers greater than 0.8. As the order of spatial differencing decreases (compare Figs. 1a, 1c, and 1e), the limit of the CFL number increases for stable calculation.

Figure 1b shows the dispersive effect of the RK3-CD6 scheme. For a CFL number of 0.4, the phase velocity is correct for wave numbers up to 1.8. The phase velocities are slower than they should be at large wave numbers. Increasing the CFL number makes phase velocities deviate from the 45^o straight line at smaller wave numbers. Decreasing the CFL number merges the curves together to reach an asymptotic curve. However, the dispersive effect at high wave numbers does not improve. Comparing Figs. 1b, 1d, and 1f shows that the increase of the order of the spatial differencing reduces the numerical dispersion at high wave numbers. Specifically, a significant improvement is achieved by changing the spatial differencing from CD2 to CD4, whereas only a limited gain is obtained by switching from CD4 to CD6.

Figure 2 shows the results of the Fourier analyses of the fourth-order Runge-Kutta (RK4) method combined with various central difference schemes. The CFL numbers are the same as that in Fig. 1. Similar to the case of RK3, for the same CFL number and wave number, e.g., CFL = 1.4, $\hat{\omega} = 1.5$, higher-order spatial discretization

introduces more artificial damping (see Figs. 2a, 2c, and 2e) and therefore reduces the CFL number limit for stable calculation. Again, the dispersive error at high wave numbers decreases as the order of the spatial differencing increases (see Figs. 2b, 2d, and 2f).

Figures. 1c and 2c can be compared to show the difference of the dissipation effects between the RK3 and RK4 methods. For the same CFL and wave numbers, the RK4 method introduces more artificial damping, and a larger CFL number could be used. On the other hand, Figs. 1d and 2d show that an increase of the order of the time marching scheme does not improve the dispersive effect at high wave numbers.

From the above discussion, it is clear that reliable solutions of the finite difference schemes are at low wave numbers. For example, for the RK4-CD6 method at CFL = 0.8 (see Figs. 2a and 2b) the solution with wave numbers less than $1/3\pi$ (6 grid nodes per wave) is fairly accurate. Numerical solutions with higher wave numbers (wave length less than 6 grid nodes) suffer significant dispersive and dissipative errors. On the other hand, for the conventional RK4-CD2 method at the same CFL, 12 to 16 grid nodes per wave are needed for an accurate solution.

It is interesting to note that compact difference schemes have no dissipative effect at the highest wave number resolved by a given numerical grid, i.e., two grid nodes per wave (see Figs. 1a, 1c, 1e, 2a, 2c, and 2e). Nevertheless, a significant dispersive error is introduced to these highest-wave-number waves and cause the even-odd decoupling of the numerical solutions. Furthermore, applying the compact difference scheme twice to calculate the viscous terms of the Navier Stokes equations does not eliminate the erroneous oscillation, owing to the linearity of the operation. These high-wave-number waves continue oscillating with erroneous phase speeds throughout the course of computation and eventually destroy the solution. It is therefore appropriate to impose a small amount of high-order artificial damping to filter out these waves while at the same time keeping the resolution at low wave modes intact. Figure 3 shows the dissipation and dispersion effects of the RK4-CD6 method at CFL=0.8 with various amounts of sixth-order artificial damping, defined as

$$\text{A.D.} = \frac{\eta}{8}[u_{i+3} + u_{i-3} - 6(u_{i+2} + u_{i-2}) + 15(u_{i+3} + u_{i-3}) - 20u_i]. \quad (35)$$

The range of η is from 0.01 to 0.05 with an increment of 0.01 between the neighboring curves. Comparison between Fig. 3 and Figs. 2a and 2b shows that no additional damping at low wave numbers is introduced into the system by the imposed artificial dissipation for $\eta \leq 0.03$, whereas the undesirable high-wave-number waves are dissipated.

2.4 Numerical Examples

2.4.1 Acoustic Admittance of A Nozzle Flow

The first case is a forced oscillatory quasi-one-dimensional flow in a converging nozzle. The governing equations are

$$\frac{\partial \mathbf{Q}}{\partial t} + \frac{\partial \mathbf{E}}{\partial x} = \mathbf{H} \tag{36}$$

where

$$\mathbf{Q} = \begin{pmatrix} \rho \\ \rho u \\ e \end{pmatrix} a, \quad \mathbf{E} = \begin{pmatrix} \rho u \\ \rho u^2 + p \\ (e+p)u \end{pmatrix} a, \quad \mathbf{H} = \begin{pmatrix} 0 \\ p\frac{da}{dx} \\ 0 \end{pmatrix}, \tag{37}$$

ρ is density, p is pressure, and e is the total energy defined as $e = \rho(C_v T + \frac{1}{2}u^2)$. C_v is the constant volume specific heat. The variable a is the cross sectional area and is prescribed as a function of x. The theoretical solution of the acoustic admittance of a choked nozzle was provided by Tsien[7] under the assumption that the velocity of the base flow is a linear function of axial location as shown in Fig. 4. The nozzle shape can be inversely derived according to Tsien's assumption, and we have

$$a = \frac{1}{M}\left(\frac{2}{\gamma+1} + \frac{\gamma-1}{\gamma+1}M^2\right)^{\frac{\gamma+1}{2(\gamma-1)}}, \tag{38}$$

where γ is the specific heat ratio and M is the Mach number which can be expressed as

$$M = \frac{x}{x^*}\sqrt{\frac{\gamma+1}{2} - \frac{\gamma-1}{2}\left(\frac{x}{x^*}\right)^2}. \tag{39}$$

The superscript $*$ denotes the property at the nozzle throat. According to Tsien's derivation, the linearized quasi-one-dimensional equations can be manipulated to the following form under the isentropic condition,

$$z(1-z)\frac{d^2P}{dz^2} - 2\left(1 + \frac{i\beta}{1+\gamma}\right)z\frac{dP}{dz} - i\beta\frac{(2+i\beta)}{2(\gamma+1)}P = 0 \tag{40}$$

$$(\gamma+1)(1-z)\frac{dP}{dz} - (\gamma - 1 + i\beta)P + (2+i\beta)U = 0 \tag{41}$$

where

$$\begin{aligned} \frac{p'}{\gamma\bar{p}} &= P(z)e^{i\beta\tau}, \\ \frac{u'}{\bar{u}} &= U(z)e^{i\beta\tau}. \end{aligned} \tag{42}$$

$\bar{u}$ and $\bar{p}$ are the velocity and pressure of the base flow, β is the normalized frequency which is defined as $\beta = \omega(1-z)/(\bar{c}^* - \bar{u})$, and τ is the non-dimensionalized time which is defined as $\tau = \bar{c}^* t/x^*$. The independent variable z can be expressed in different forms due to the linearity between the base flow velocity $\bar{u}$ and axial location x, and we have

$$
\begin{aligned}
z &= \frac{x}{x^*} \\
&= \frac{\bar{u}}{c^*} \\
&= \frac{(\gamma+1)M^2}{2+(\gamma-1)M^2}
\end{aligned}
\tag{43}
$$

With Eqn. (43), it is clear that P and U are functions of the Mach number (M) with prescribed frequency (β). Equation (40) is a hypergeometric equation[14] that can be solved by a power series expansion. The converged solution does not exist in the supersonic region because the Mach number is greater than unity. $U(z)$ can be easily solved with $P(z)$ known as shown in Eqn. (41). Finally, the acoustic admittance function defined as $A(z) = U(z)/P(z)$ can be obtained as a function of the Mach number.

In what follows, the procedure of the CFD calculation to compare with Tsien's solution is illustrated. First, the base flow field is obtained by solving the quasi-one-dimensional equations, Eqns. (36) and (37), using the RK4-CD2 method with the nozzle area ratio prescribed by Eqns. (38) and (39). The results are checked by the area Mach number relation[15] and the solution is accurate up to five decimal digits. The perturbation at the inlet is obtained by specifying sinusoidal pressure fluctuations in terms of magnitude and frequency. With the prescribed pressure and isentropic correlation, the temperature fluctuation is also determined. Numerically, these boundary conditions are enforced by defining a vector $\mathbf{k} = \mathbf{k}(\mathbf{Q})$ at the upstream boundary, such as

$$
\mathbf{k} = \begin{pmatrix} p \\ T \\ 0 \end{pmatrix} = \begin{pmatrix} \xi_1 \\ \xi_2 \\ 0 \end{pmatrix}, \tag{44}
$$

where ξ_1 and ξ_2 are the specified values of p and T. To proceed, Equation (44) is linearized to become a function of $\Delta\mathbf{Q}$, such as

$$
\mathbf{k^{n+1}} = \mathbf{k}^n + \frac{\partial \mathbf{k}}{\partial \mathbf{Q}} \Delta \mathbf{Q}, \tag{45}
$$

where $\mathbf{k^{n+1}}$ is equal to the specified pressure and temperature at the time step $n+1$ and $\partial\mathbf{k}/\partial\mathbf{Q}$ is a 3×3 matrix. In order to close the system, the null entry in the vector $\mathbf{k}$ may be filled by the out-running characteristic relation deduced from the flow equations. Numerically, the similarity transformation is applied to the discretized flow equations (see Eqn. (4)), and we get

$$
\begin{gathered}
\mathbf{L}\mathbf{M}^{-1}(\mathbf{Q}^i - \mathbf{Q}^n) = \mathbf{L}\mathbf{M}^{-1}\Delta t \sum_{k=1}^{i} \alpha_{ik}\mathbf{R}^{k-1}, \\
i = 1, \cdots, N
\end{gathered}
\tag{46}
$$

where $i = 1, \cdots, N$ represents the N-step RK method. Here, $\mathbf{M}^{-1}$ is the eigenvector matrix of Jacobian matrix $\mathbf{A} = \partial\mathbf{E}/\partial\mathbf{Q}$, and $\mathbf{L}$ is a selection matrix with zeros and ones on the diagonal in such a fashion that the proper outrunning characteristics are selected. By combining the imposed conditions, Eqn. (45), with the outrunning characteristic relations, Eqn.(46), we form the complete equation at the boundary point as,

$$\left(\mathbf{L}\mathbf{M}^{-1} + \frac{\partial \mathbf{k}}{\partial \mathbf{Q}}\right)(\mathbf{Q}^i - \mathbf{Q}^n) = \mathbf{L}\mathbf{M}^{-1}\Delta t \sum_{k=1}^{i} \alpha_{ik}\mathbf{R}^{k-1} + \mathbf{k}^{n+1} - \mathbf{k}^n, \qquad i = 1, \cdots, N \tag{47}$$

For the supersonic out-flow condition, Eqn. (46) is used with the selection matrix $\mathbf{L}$ equal to an identity matrix. In both cases, the out-running characteristic equations are solved with one-sided difference as shown in Eqn. (14). In other words, the characteristic boundary conditions are always discretized by an upwinding scheme which is physically sound and the numerical stability is enhanced. These boundary conditions are applied at each of the Runge-Kutta stages.

The acoustic admittance is a complex number and can be written as $A = |A|e^{i\theta}$. In the present paper, a small pressure perturbation of 1.1% ($p' = 0.011\bar{p}$) is imposed at the nozzle inlet. The length of the converging part of the nozzle is 0.9 L^* (see Fig. 4) and the inlet Mach number is about 0.09. The frequency of the perturbation is set at $\beta = 6$, which corresponds to about 2000 Hz.

Figure 5 shows the comparisons between the CFD results of the RK4-CD6 method and the theoretical solution of the acoustic admittance in terms of the magnitude $|A|$ and the phase angle θ in the subsonic region of the nozzle. Both the magnitude and the phase angle of the acoustic admittance decrease as the flow speeds up. As shown in the figure, perfect agreement is obtained for the comparison of $|A|$, while the predicted phase angle is slightly off due to the resolution of the numerical grid for the phase angle. In this case, the harmonic content of the solution is limited to one frequency with a wave length comparable to the computational domain which is resolved by 61 grid nodes. Therefore, all numerical schemes of concern provide accurate solutions. The numerical errors of $|A|$ and θ are tabulated in Table 2. There is slight advantage in using the higher-order schemes for the prediction of $|A|$; however, no obvious advantage of using the higher-order scheme for the phase angle calculation is observed.

2.4.2 Shocked Sound Waves

The second case is the propagation of shocked sound waves in a tube with a periodic boundary condition. The governing equations are the same as in the first case, namely, Eqns. (36) and (37), with cross section area (a) equal to a constant. This case is interesting for its complex harmonic content compared to the first case. In addition, the capability of the high-order compact difference schemes for

shock capturing can also be studied. At time equal to zero, a sinusoidal pressure distribution is given. Because of the periodic boundary condition, only one cycle resolved by 61 grid nodes is imposed in the computational domain. According to the isentropic condition, the distributions of temperature, density, and speed of sound are also determined. The velocity profile is determined by the simple wave correlation[16], such as

$$\begin{aligned} u(x) &= \int_{\bar{p}}^{p(x)} \frac{dp}{\rho(x)c(x)}, \\ &= \frac{2\gamma}{\gamma-1}\sqrt{\frac{\bar{p}^{\frac{1}{\gamma}}}{\gamma\bar{\rho}}}\left(p(x)^{\frac{\gamma-1}{2\gamma}} - \bar{p}^{\frac{\gamma-1}{2\gamma}}\right), \end{aligned} \tag{48}$$

where the average flow properties are denoted by a bar. With the simple wave correlation, the wave forms of all flow properties are in phase and the initial condition of the present CFD computation matches the theoretical analysis provided by Morse and Ingard[8]. It is interesting to note that the simple wave correlation is an extension of a linear, plane, acoustic wave. For a variation of pressure less than 5%, the plane wave relations could be adopted, such as

$$\begin{aligned} T(x) &= \bar{T}\left(1 + \frac{\gamma-1}{\gamma}\frac{p'(x)}{\bar{p}}\right), \\ \rho(x) &= \bar{\rho}\left(1 + \frac{p'(x)}{\gamma\bar{p}}\right), \\ u(x) &= c(x)\frac{p'(x)}{\gamma\bar{p}}, \end{aligned} \tag{49}$$

where $p'(x)$ is the prescribed pressure fluctuation. As shown in Eqns. (48) and (49), the wave speeds $u+c$, $u-c$ and u vary as a result of the flow property distribution. The distortion of the wave form is a cumulative effect resulting from the wave speed distribution. For simple waves, i.e., all flow properties are in phase, the wave crest will quickly overtake the trough and form a shock.

Figure 6 shows the time history of the pressure fluctuation at one end of the computational domain for various finite difference schemes. According to Morse and Ingard, the first shock appears after about two cycles for the case of a 10% pressure perturbation ($p'/\bar{p} = 0.1$)[8]. All schemes of concern predict the wave steepening rate correctly. After the wave shocked, the flow evolution is no longer isentropic and the kinetic energy is gradually converted to thermal energy due to the existence of the shock wave. As a result, the strength of the shock wave diminishes as time passes.

The shock front is a combination of many wave modes travelling at the same speed. The dispersion error introduced by the finite difference schemes will cause the high-wave-number waves to travel with erroneous speeds. As shown in Fig. 6, the methods of RK4-CD6 and RK4-CD4 with a small amount of the sixth-order artificial damping ($\eta = 0.02$) crisply resolve the shock except for the over-shoots.

These over-shoots are caused by the Gibbs phenomenon and can be fixed only by TVD type shock-capturing schemes. Almost no difference can be observed between the results of the CD4 and CD6 methods. On the other hand, the method of RK4-CD6 without background filtering shows that significant high-wave-number waves lag behind the shock front because the compact difference scheme introduces no dissipative but high dispersive effects on the highest wave number waves. As shown in the figure, these oscillations eventually contaminate the whole solution. For the conventional RK4-CD2 method, results show significant oscillations of moderate wave numbers behind the shock front because of dispersion errors.

Figure 7 shows the normalized power spectrums of the pressure profiles after about 17 cycles calculated by different methods. The analytical solution is plotted as the solid line. The power of each wave mode is roughly inversely proportional to the square of the wave number ($\propto 1/n^2$). Since 61 grid nodes are used, only 30 Fourier modes are resolved for the power spectrum (the other 30 modes are the complex conjugates). Clearly, the method of RK4-CD2 has significant errors in low wave modes. On the other hand, the methods of RK4-CD4 and RK4-CD6 compare well with the analytical solution.

2.4.3 Vortex Propagation in an Uniform Flow

A Lamb vortex propagated in an uniform flow is chosen as a two-dimensional numerical example. The vortex can be characterized by the circulation Γ and the core radius a. The azimuthal velocity u_θ at a distance r from the vortex center is given as,

$$u_\theta = \frac{\Gamma}{2\pi}\frac{r}{r^2+a^2}, \tag{50}$$

The flow near the vortex center is a rigid-body rotation ($u_\theta \propto r$). The flow far outside the core is irrotational ($u_\theta \propto 1/r$) with u_θ decreasing as r increases. Eqn. (50) is a continuous function to connect the two extremes. With the prescribed velocity field, the pressure and density distributions of the vortex can be determined by the momentum and the energy equations,

$$\frac{\partial p}{\partial r} = \rho\frac{u_\theta^2}{r}, \tag{51}$$

$$\frac{\gamma}{\gamma-1}\frac{p}{\rho} + \frac{u_\theta^2}{2} = h_o, \tag{52}$$

where h_o is the total enthalpy and is set to be a constant such as $h_o = \gamma\bar{p}/(\gamma-1)\bar{\rho}$ with the free stream condition denoted by a bar. To proceed, substitute Eqns. (50) and (52) into Eqn. (51) and integrate the equation over r. As a result, the pressure distribution is obtained. Consequently, the density distribution and the whole flow field is determined. The solutions of this stationary vortex can be superimposed to any uniform flow with arbitrary speed. Physically, this process may be interpreted as a stationary vortex being observed from a moving coordinate system with constant velocity. Thus, the vortex in an uniform flow can be constructed as,

$$u = \bar{u} + u',$$
$$v = \bar{v} + v', \tag{53}$$

where the velocities of the background flow are denoted by a bar and the superscript $'$ denotes the vortex velocities specified by Eqn. (50). The pressure and density distribution of the moving vortex is the same as that of the stationary vortex and may be obtained from the solutions of Eqns. (51) and (52).

The boundary condition of the present case is an extension of the characteristic type treatment discussed in Case 1. Essentially, only one-dimensional characteristics (derived from two-dimensional flow equations) normal to the computational boundary are considered. For the purposes of this discussion, the subsonic out-flow condition is considered. The coupled equations of three out-running characteristics and one specified boundary condition, similar to that in Eqn. (47), should be solved. For steady state calculations, a back pressure (p_b) is specified to regulate the flow rate, such as

$$\mathbf{k} = \begin{pmatrix} 0 \\ 0 \\ 0 \\ p_b \end{pmatrix} \tag{54}$$

Similarly, the dimension of vectors $\mathbf{Q}$ and $\mathbf{R}$ is four and the matrix $\mathbf{M}^{-1}$ is a 4×4 eigenvector matrix for the flux vector normal to the computational boundary.

For a non-reflective boundary condition, Giles' formulation[17] instead of the back pressure is used to fill the entry for the specified boundary condition, such as

$$\frac{\partial c_4}{\partial t} + (0, u, 0, v)\frac{\partial}{\partial y}\begin{pmatrix} c_1 \\ c_2 \\ c_3 \\ c_4 \end{pmatrix} = 0 \tag{55}$$

where y is in the direction parallel to the computational boundary. The variables $c_i, i = 1, \cdots, 4$ are the characteristic variables and can be obtained by the similarity transformation from the non-conservative form equations as illustrated by Giles. In our case, the characteristic variables are derived from the conservative-form equations using the same eigenvector matrix $\mathbf{M}^{-1}$ as in the aforementioned discussion. Giles' non-reflective formulation, Eqn. (55), is relatively simple to used with an existing one-dimensional characteristic boundary condition. Nonetheless, according to Giles' analysis, some two-dimensional effect is considered in the equation. Numerically, Eqn. (55) may be discretized according to the finite difference scheme of the interior nodes and combined with the discretized out-running characteristic equations (the two-dimensional version of Eqn. (46)) to form the complete subsonic out-flow boundary condition. It is interesting to note, however, according to Huff's study[18] and our experience, that stretching the numerical grid nodes downstream to dampen the outgoing unsteady waves is just as effective.

For the in-flow conditions, the characteristic-type treatment combined with Giles' equation (different from Eqn. (55)) may be adopted. For the present calculations, however, the upstream condition is relatively insensitive to various forms of non-reflective treatment as long as the proper out-running characteristic equation is selected and solved with the prescribed incoming conditions similar to that in Eqn. (47). In the present case, constant total pressure and total temperature are prescribed as the forcing boundary conditions upstream.

As in the one-dimensional cases, dissipative and dispersive effects of various schemes are assessed. The prescribed vortex flow field contains a broad band of frequencies due to the distribution of the azimuthal velocity. Theoretically, all wave modes travels at the same speed to ensure the integrity of the vortex structure. For numerical methods with dispersive error, the shape of the vortex could deform, even break up in the later stage of the time marching procedure. In addition, the dissipation effect of finite difference schemes can be evaluated by the conservation of the sharp pressure dip at the center of the vortex propagated in the numerical grid.

In the present calculations, the Mach number of the background flow is 0.4. The grid size is 301 $\times$ 91 in the streamwise and transverse directions, respectively. Uniform grids are used in the axial direction and the transverse grids are stretched near the outside boundary. The CFL number calculated based on the background flow is about 0.7 for all calculations. As discussed before, a small amount of background filtering ($\eta = 0.02$) is applied for all calculations. The core radius (a) is about 1 cm and is resolved by about 4 grid nodes.

Figure 8 shows the vorticity and Mach number contours of the initial condition prescribed by Eqns. (50) - (53). Figure 9 shows the contours after the eddy propagates about 60 core radii downstream as simulated by various numerical schemes. The comparison between Fig. 8 and Fig. 9 shows that the structure of the eddy is retained by the compact difference schemes (CD4 and CD6). In contrast, the eddy predicted by the second-order central difference is shattered due to the excessive dispersive error.

Figure 10 shows pressure distributions of the eddy at various instances. In this figure, the x axis represents the streamwise locations non-dimensionalized by the core radius of the vortex and the y axis is the pressure. For both CD4 and CD6 methods, the pressure at the vortex center increases about 1 % through the process. In comparison, the results of the second-order scheme show pressure fluctuations with an overall increase about 3 %. The pressure fluctuation predicted by the second-order scheme is due to the deviation of the vortex path.

2.4.4 Vortex Pairing

Finally, the calculation of the single vortex is extended to the simulation of the vortex pairing. The vortex pairing is the controlling mechanism for the growth of the mixing layer[10]. In theory, vortex pairing occurs when the distance between two vortices is less than a threshold value. Unfortunately, no theoretical analysis

is available for compressible flows. In the present paper, the RK4-CD6 method is used to simulate the pairing process to demonstrate the resolution of the high-order compact difference scheme.

The initial condition is specified by two identical vortices placed 5 core radii apart in a quiescent gas. The core radius is 1 cm and circulation is 15 m^2/s. At the center of each vortex, there is a pressure deficit about 15% compared to the ambient gas. The grid size is 201×201. Uniform grids are used at the center of the computational domain to resolve the vortices. The grids are slightly stretched in all four directions to prevent erroneous wave reflection. In addition, one-dimensional characteristic equations combined with Giles' unsteady, subsonic, out-flow equation is solved on the boundary as the non-reflective boundary condition.

Figure 11 shows the contours of the vorticity magnitude at various stages of the vortex interaction. The whole sequence is about one and a half revolutions. Finally, a single larger vortex emerges as the result of the vortex pairing interaction. Figure 12 shows the corresponding Mach number contours for the same flow.

3. Concluding Remarks

In this work, the quasi-one-dimensional and two-dimensional Euler solvers using various combinations of the Runge Kutta methods and the compact difference schemes were developed for numerical simulations of unsteady flows. The accuracy of the finite difference schemes is assessed by Fourier analysis and numerical examples in terms of numerical dissipation and dispersion. The dispersive characteristic is improved by high-order compact difference schemes compared to the second-order central difference. The increase of the order of time stepping scheme, on the other hand, enlarges the CFL limit for stable computations. In particular, significant improvement of the dispersive effect is obtained by adopting the fourth-order compact scheme (6 to 8 grid nodes to resolve a wave) instead of the conventional second-order central difference (12 to 16 grid nodes for one wave). The use of the sixth-order compact scheme (5 to 8 grid nodes for one wave), however, gains little improvement compared with the fourth-order scheme. It was also found that the compact difference schemes have no dissipative but high dispersive effects to the highest-wave-number waves resolved by a given numerical grid. Consequently, a small amount of background filtering is necessary to dissipate the high-wave-number waves and, at the same time, keep the low-wave-number solution intact. Other issues such as the order of accuracy of the Runge-Kutta schemes for nonlinear equations are analyzed. Specifically, the criteria for the 3 and 4-step methods to be third and fourth-order accurate are derived. The accuracy of the compact difference schemes for the steady state solution is also addressed.

In general, simulation of unsteady flow provides an overwhelming amount of information. It is our experience that the initial and boundary conditions must be carefully set up to obtain interpretable and physically meaningful solutions. For practical purposes, Giles' non-reflective equations combined with one-dimensional characteristic equations and their implementation to the present numerical scheme

were illustrated in detail. In addition, the initial conditions of the simple wave, plane acoustic wave, and the Lamb vortex were also provided. Finally, as illustrated in the numerical examples, for flows of simple harmonic content, e.g., one frequency in Case 1, the conventional second-order central difference scheme is adequate provided enough grid nodes are used to resolve the very wave mode. On the other hand, for flows of complex harmonic content, the use of the Runge-Kutta method combined high-order compact difference schemes shows crisp resolution of unsteady flows.

4. References

[1] Lele, S. "Direct Numerical Simulations of Compressible Free Shear Flows," AIAA Paper 89-0374 (1989).

[2] Lele, S. "Compact Finite Difference Schemes with Spectral-Like Resolution," CTR Manuscript 107, Center for Turbulence Research, Stanford University, C. A. (1990).

[3] Jameson, A., Schmidt, W. and Turkel, E. "Numerical Solutions of the Euler Equations by Finite Volume Methods Using Runge-Kutta Time-Stepping Schemes," AIAA Paper 81-1259 (1981).

[4] Jameson, A. and Baker, T. J. "Solution of Euler Equations for Complex Configuration," AIAA Paper 83-1929 (1983).

[5] Wray, A. A., "Very Low Storage Time Advancement Schemes," *Internal Report*, NASA Ames Research Center, Moffett Field, C. A. (1986).

[6] Ciment, M., Leventhal, S. H., and Weinberg, B., *J. Comput. Phys.* **28**, 135 (1978).

[7] Tsien, H. S., *J. Am. Rocket Soc.* **22**, 139 (1952).

[8] Morse, P. M. and Ingard, K. U., "Theoretical Acoustics," *McGraw-Hill*, 874 (1968).

[9] Liu, N.-S., Davoudzadeh, F., Briley, W. R., and Shamroth, S. J., *J. Fluids Eng.* **12**, 501 (1990).

[10] Winant, C. D. and Browand, F. K., *J. Fluid Mech.* **63**, 237 (1974).

[11] Carnahan, B., Luther, A. A., and Wilkes, J. O., "Applied Numerical Methods," *John Wiley & Sons, Inc.*, 363 (1969).

[12] Colatz, L., "The Numerical Treatment of Differential Equations," *Springer Verlag*, 538 (1966).

[13] Adam, Y., *J. Comput. Phys.* **24**, 10 (1977).

[14] Williams, F. A., "Combustion Theory" *Benjamin & Cummings*, 306 (1985).

[15] Anderson, J. D., "Modern Compressible Flow," *McGraw-Hill*, 128 (1982).

[16] Lighthill, J., "Waves in Fluids," *Cambridge University Press*, 142 (1978).

[17] Giles, M. B., *AIAA J.* **28**, 12, 2050 (1990).

[18] Huff, D. L., "Pressure Waves Propagation Studies for Oscillating Cascades," NASA-TM-105406 (1992).

Table 1. The Accuracy of the 3-Step Runge-Kutta Methods.

Δt	Expansion	3-step R-K methods
0	R	R
1	R	$(\alpha_{31}+\alpha_{32}+\alpha_{33})R$
2	$\frac{1}{2}RR'$	$[\alpha_{11}\alpha_{32}+\alpha_{33}(\alpha_{21}+\alpha_{22})]RR'$
3	$\frac{1}{6}(R^2R''+RR'^2)$	$\frac{1}{2}[\alpha_{11}^2\alpha_{32}+(\alpha_{21}+\alpha22)^2\alpha_{33}]R^2R''$ $+\alpha_{11}\alpha_{22}\alpha_{33}RR'^2$

Table 2. The Relative Error of the Acoustic Admittance Calculation (%).

Numerical Schemes	Error of $\|A\|$	Error of θ
RK4-CD6	0.45	3.6
RK4-CD4	0.52	3.3
RK4-CD2	1.65	4.1

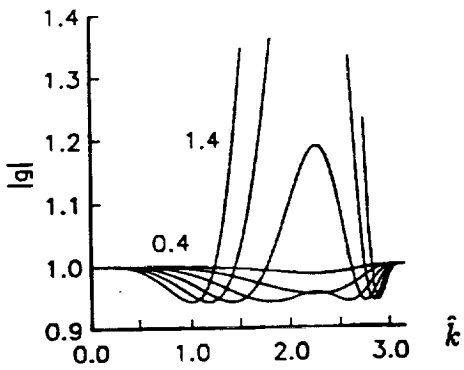

a. Dissipation of RK3–CD6

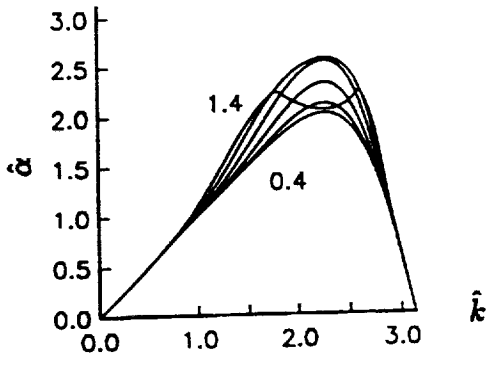

b. Dispersion of RK3–CD6

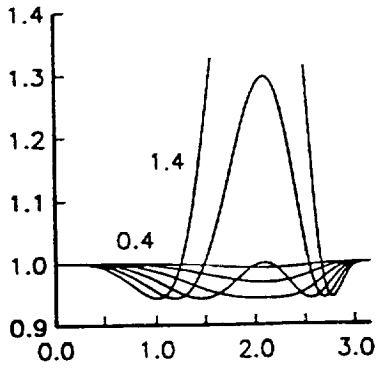

c. Dissipation of RK3–CD4

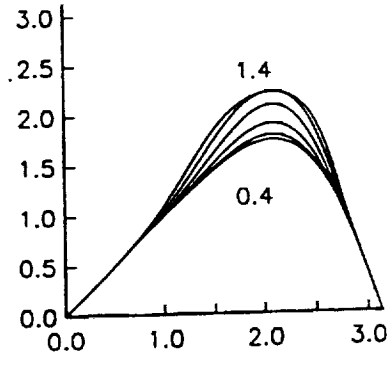

d. Dispersion of RK3–CD4

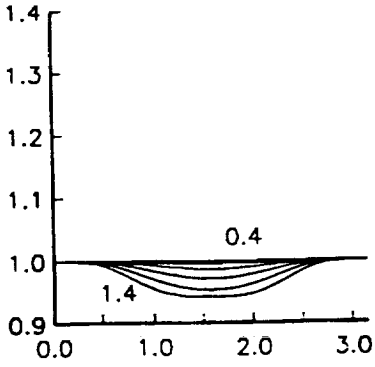

e. Dissipation of RK3–CD2

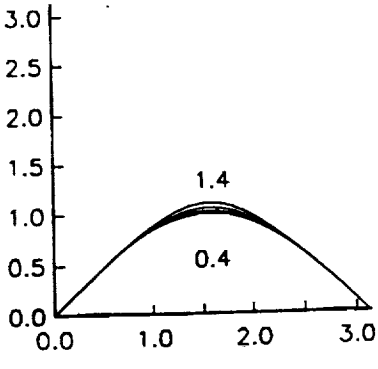

f. Dispersion of RK3–CD2

Fig. 1 Dissipation and dispersion characteristics of the RK3 time-stepping combined with various spatial discretization schemes.

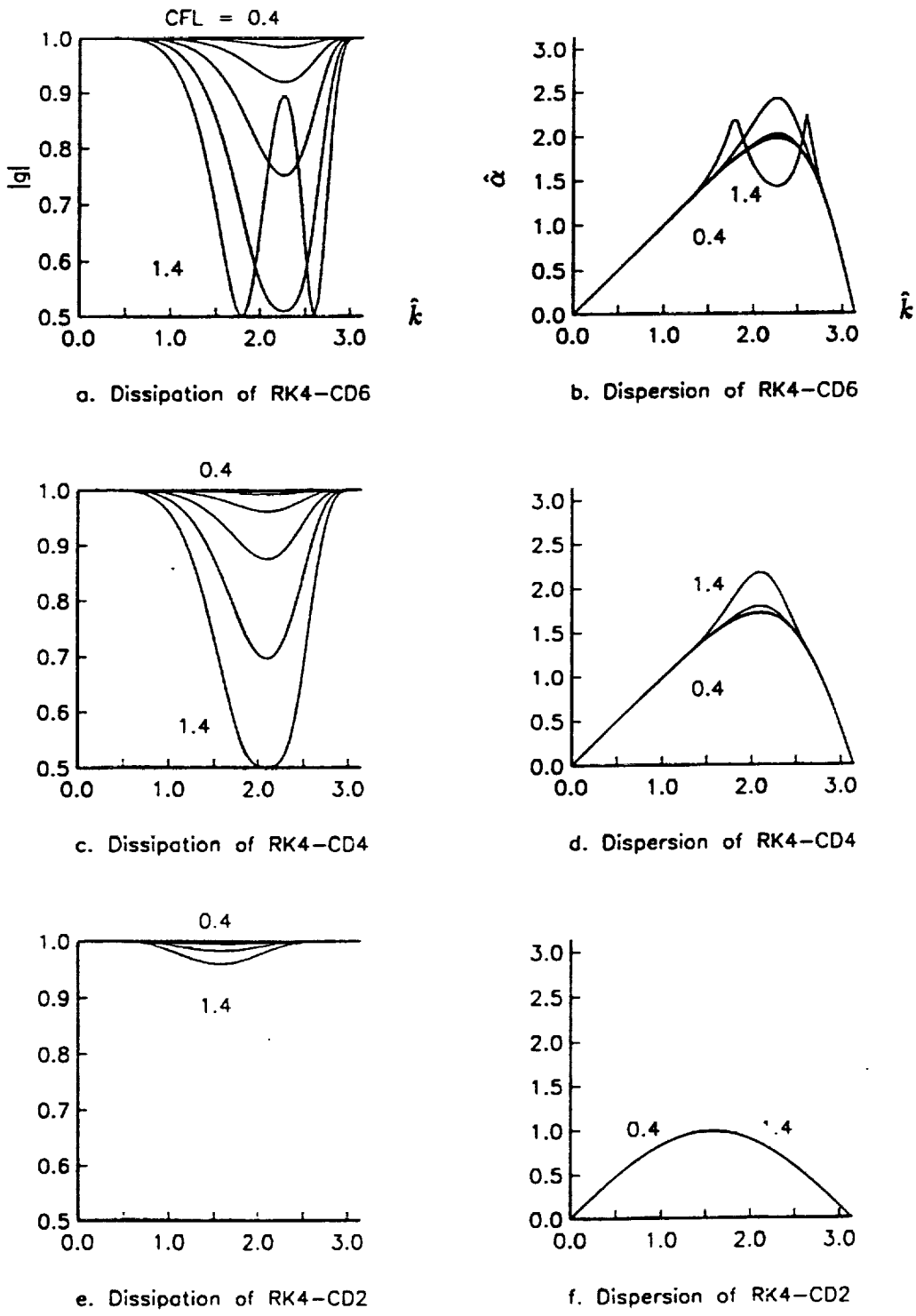

Fig. 2 Dissipation and dispersion characteristics of the RK4 time-stepping combined with various spatial discretization schemes.

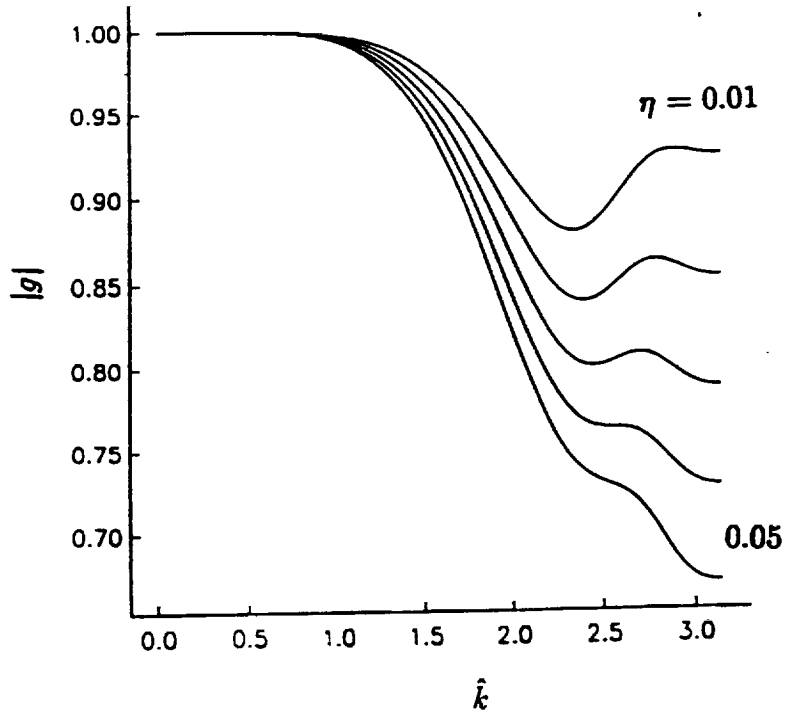

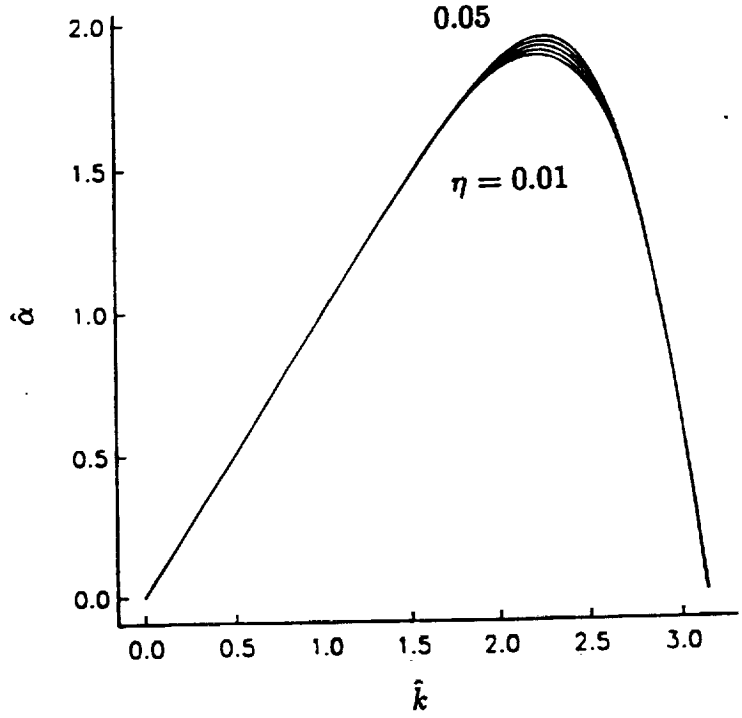

Fig. 3 Dissipation and dispersion characteristics of the RK4-CD6 method with various amount of the sixth-order numerical damping.

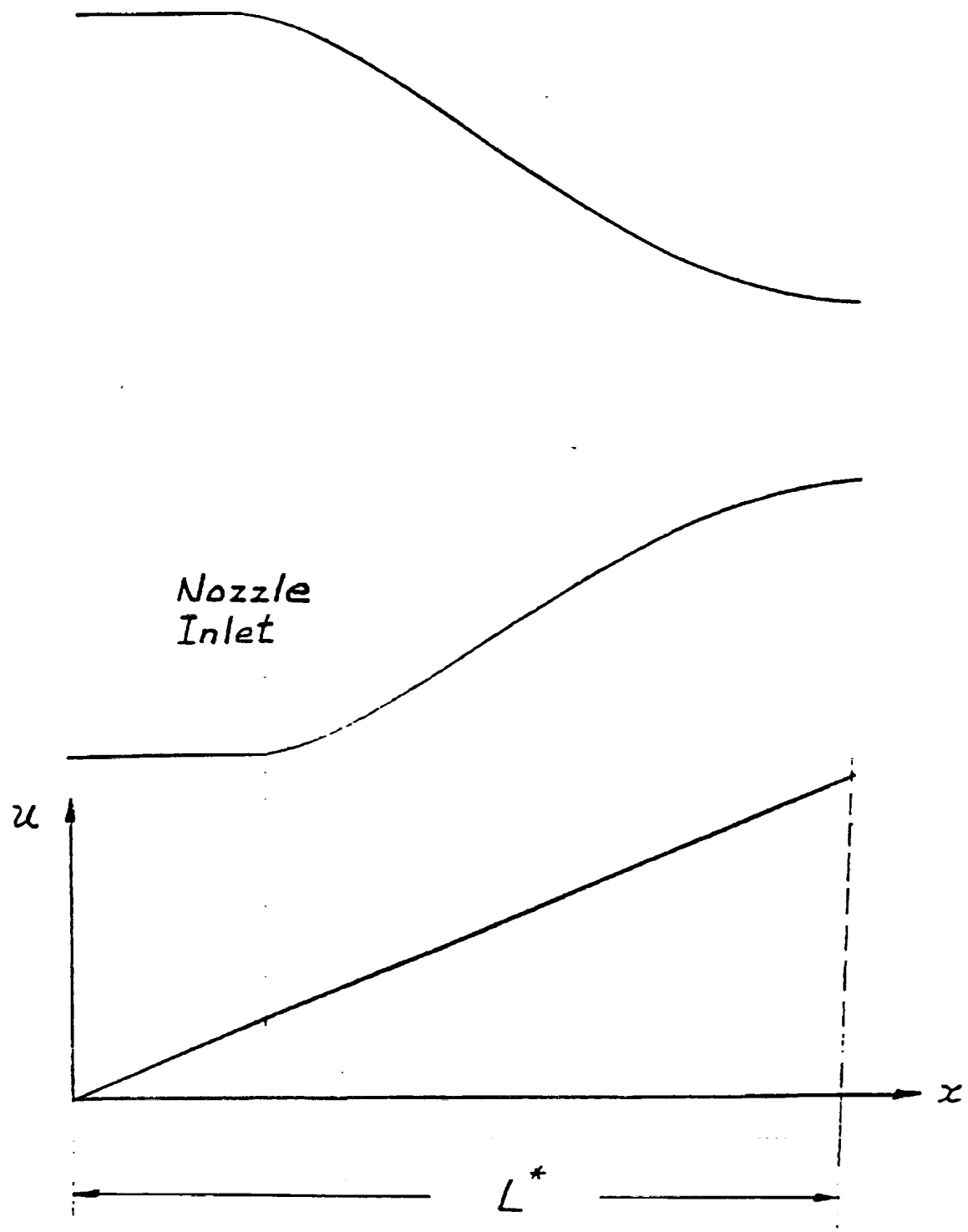

Fig. 4 Configuration of Tsien's converging-diverging nozzle [7].

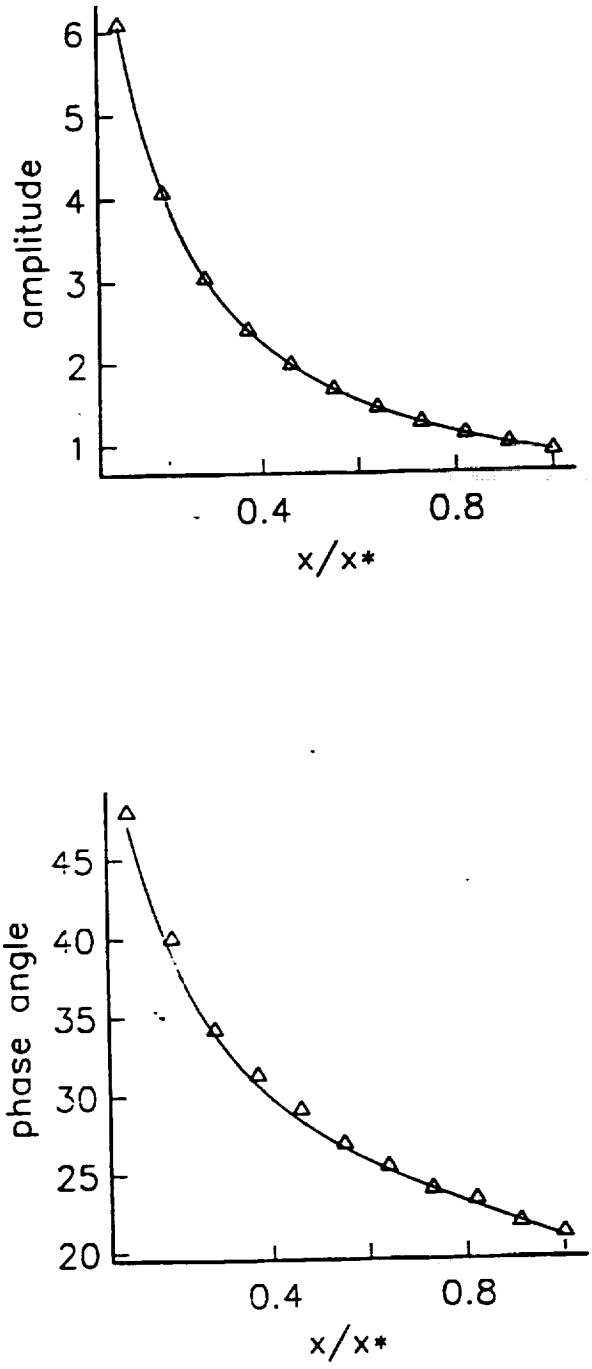

Fig. 5 Acoustic admittance calculation using the RK4-CD6 method for the inlet perturbation as $\beta = 6$, $p'/\bar{p} = 0.011$. The solid line is Tsien's theorem and the triangles are the CFD results. (a) Magnitude. (b)Phase angle.

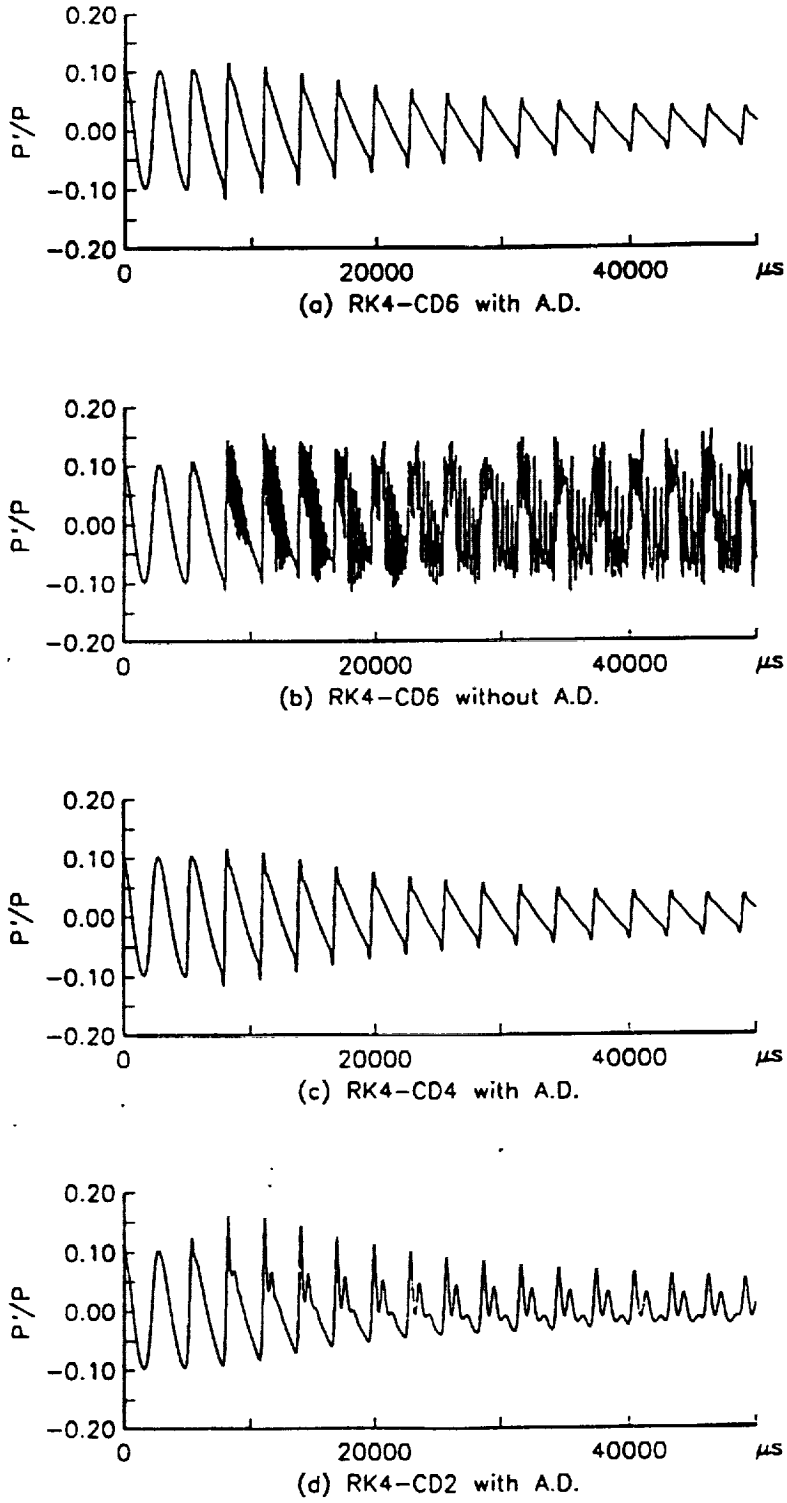

Fig. 6 Time histories of the pressure fluctuations of the N-wave calculation at one end of the periodic domain by various numerical schemes.

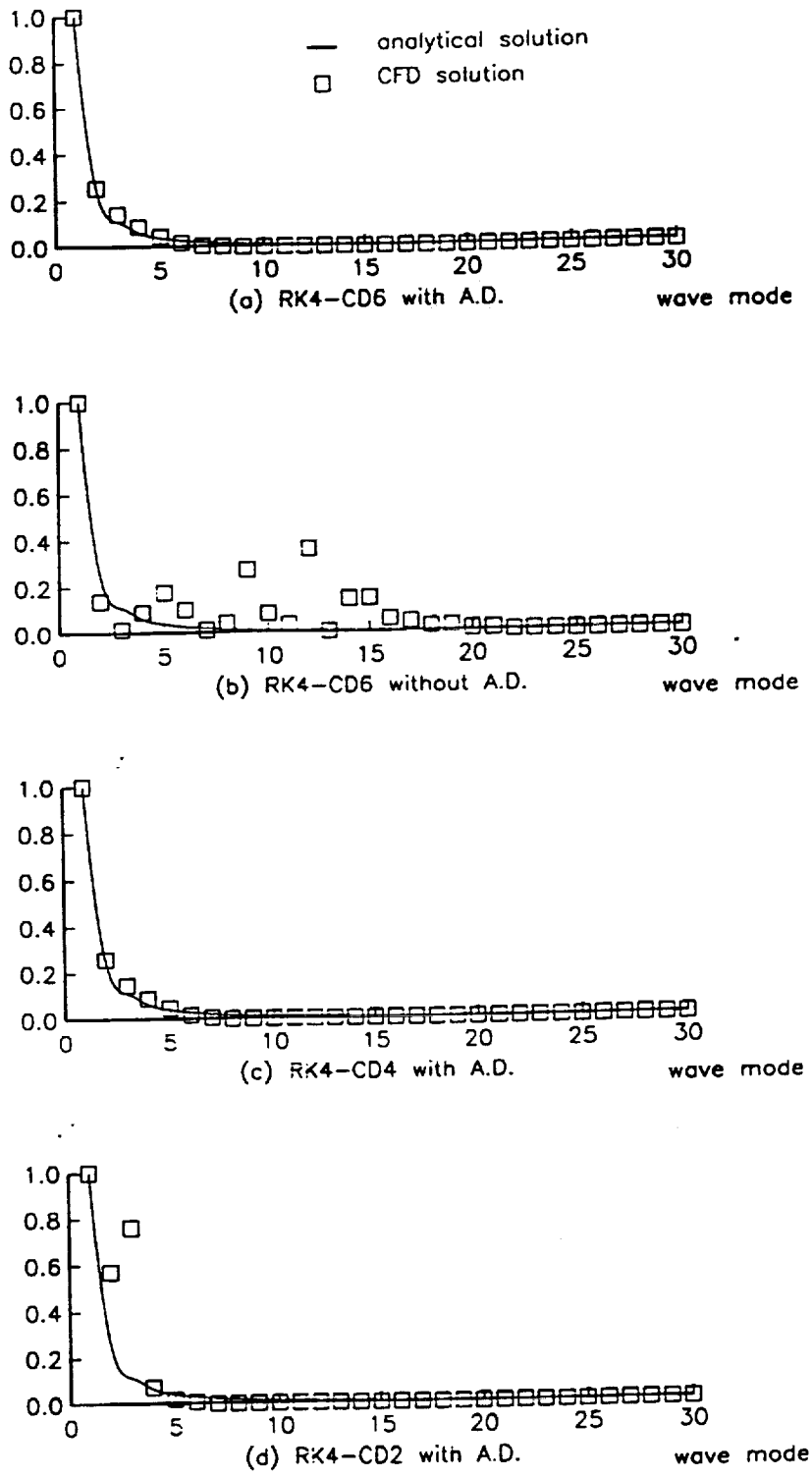

Fig. 7 Power spectrum of the pressure distribution after about 17 cycles of the N-wave propagation by various numerical schemes.

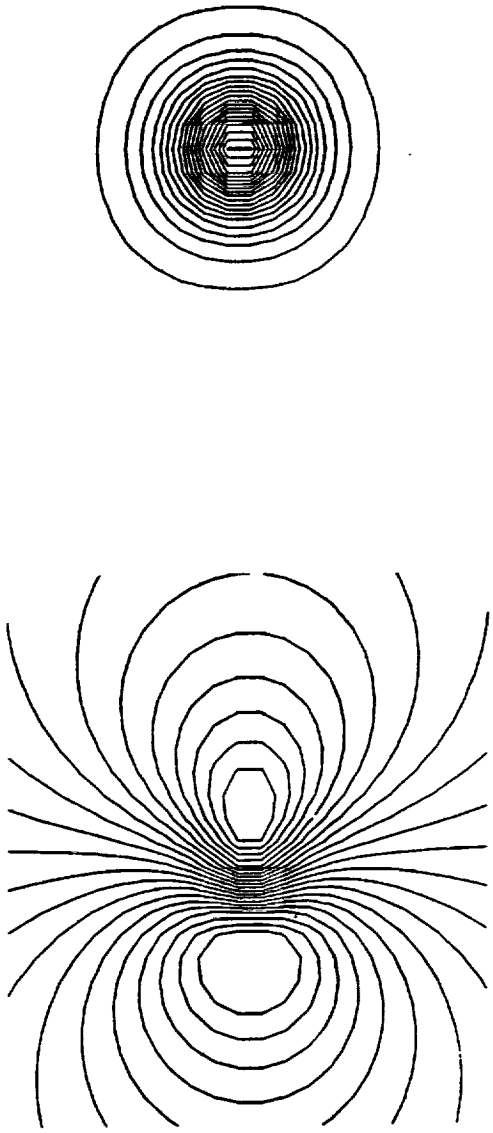

Fig. 8 Vorticity and Mach number contours of an analytical Lamb vortex.

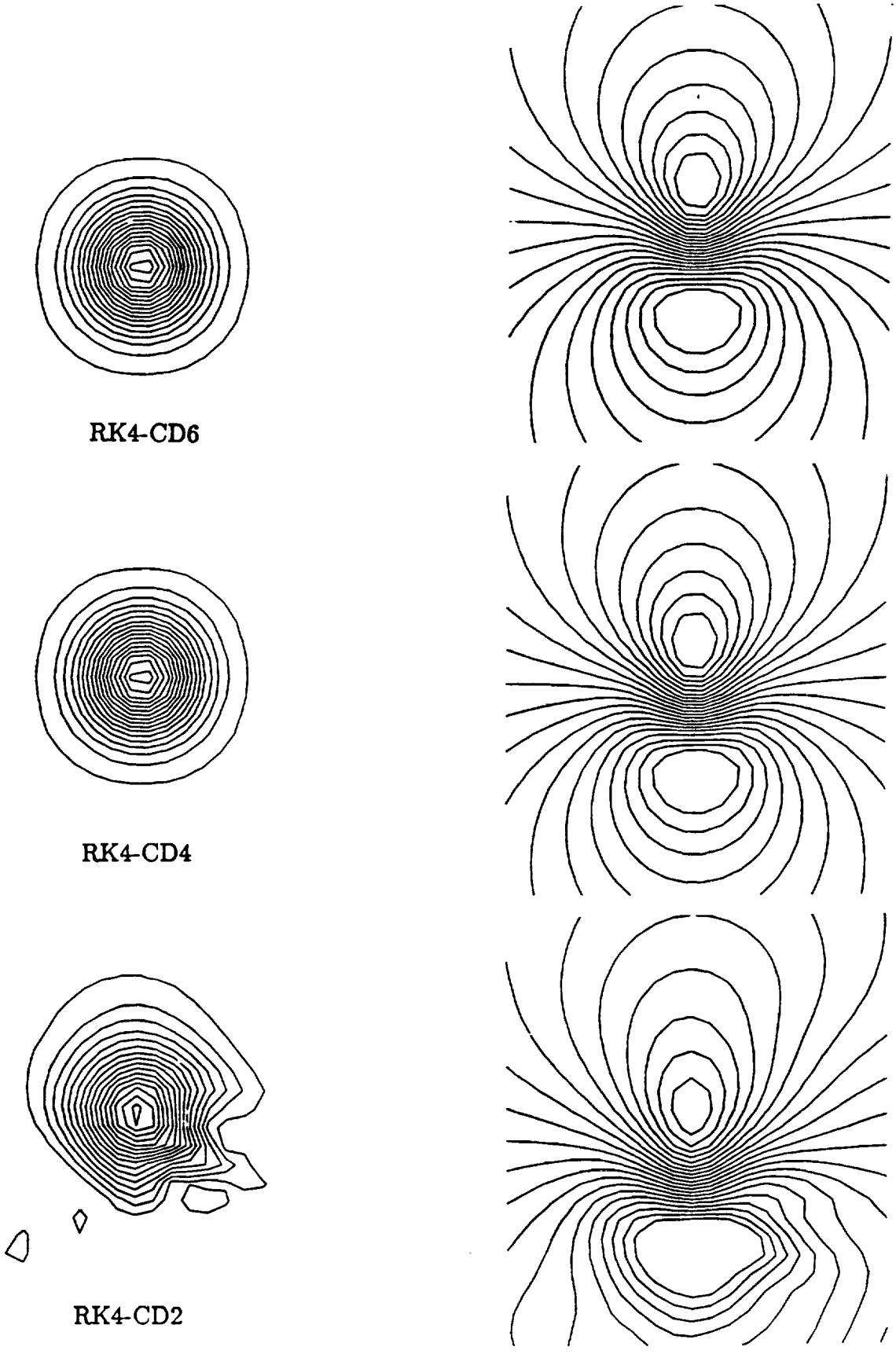

Fig. 9 Vorticity and Mach number contours of the lamb vortex after travelling about 60 core diameters predicted by various numerical schemes.

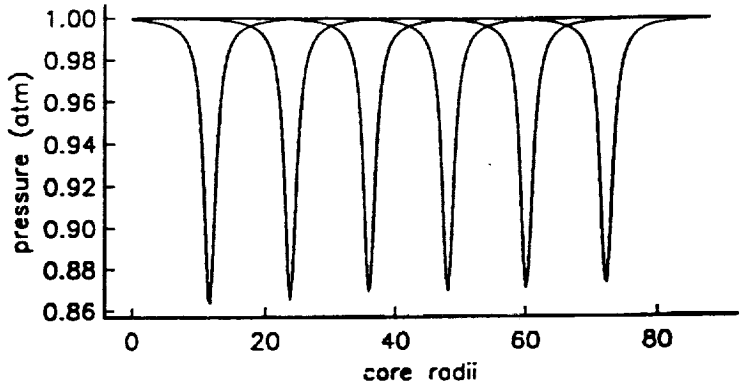

a. RK4−CD6

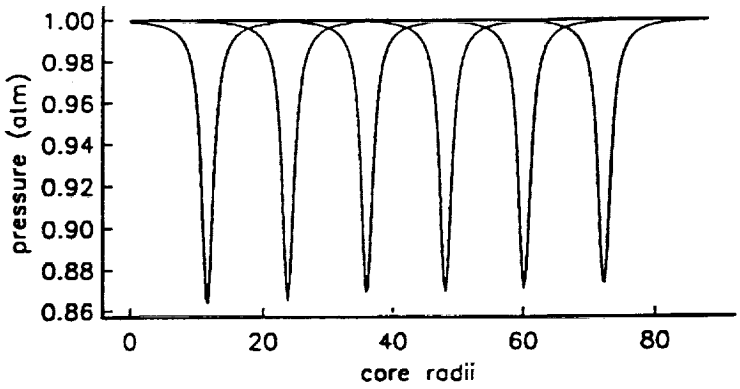

b. RK4−CD4

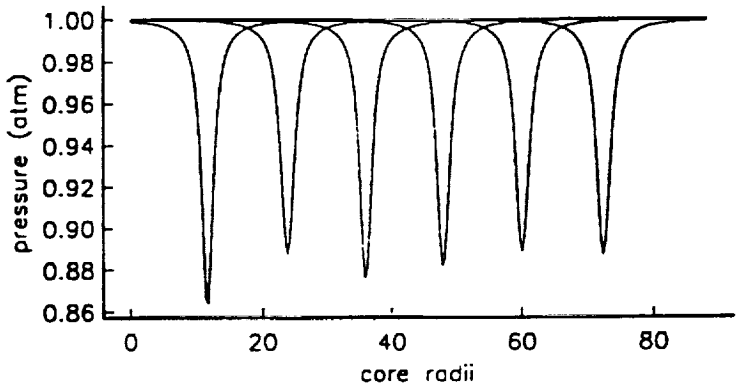

c. RK4−CD2

Fig. 10 Vortex pressure profiles at the center line at various instances predicted by different numerical schemes

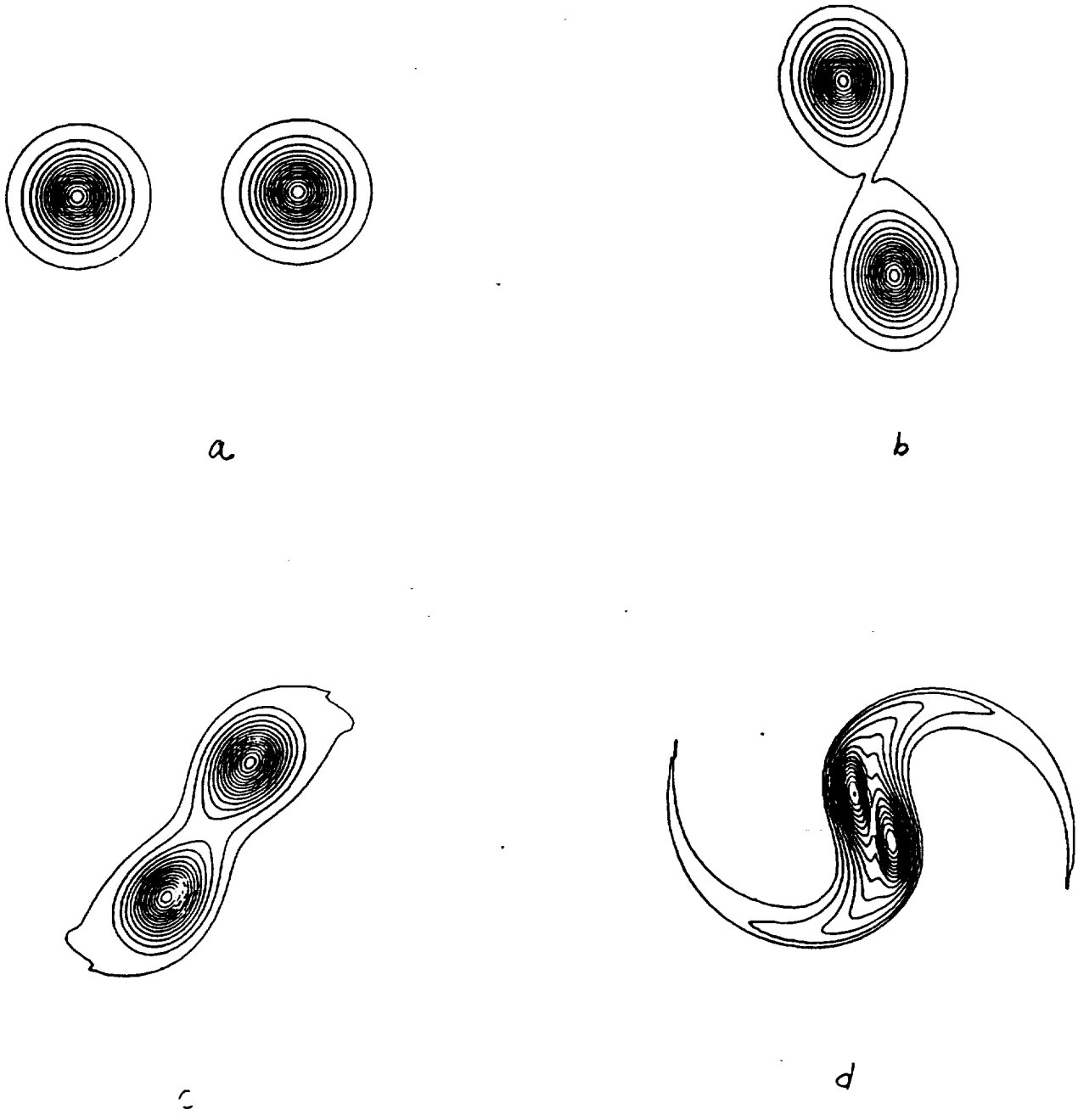

Fig. 11 The vorticity magnitude contours for the vortex pairing.

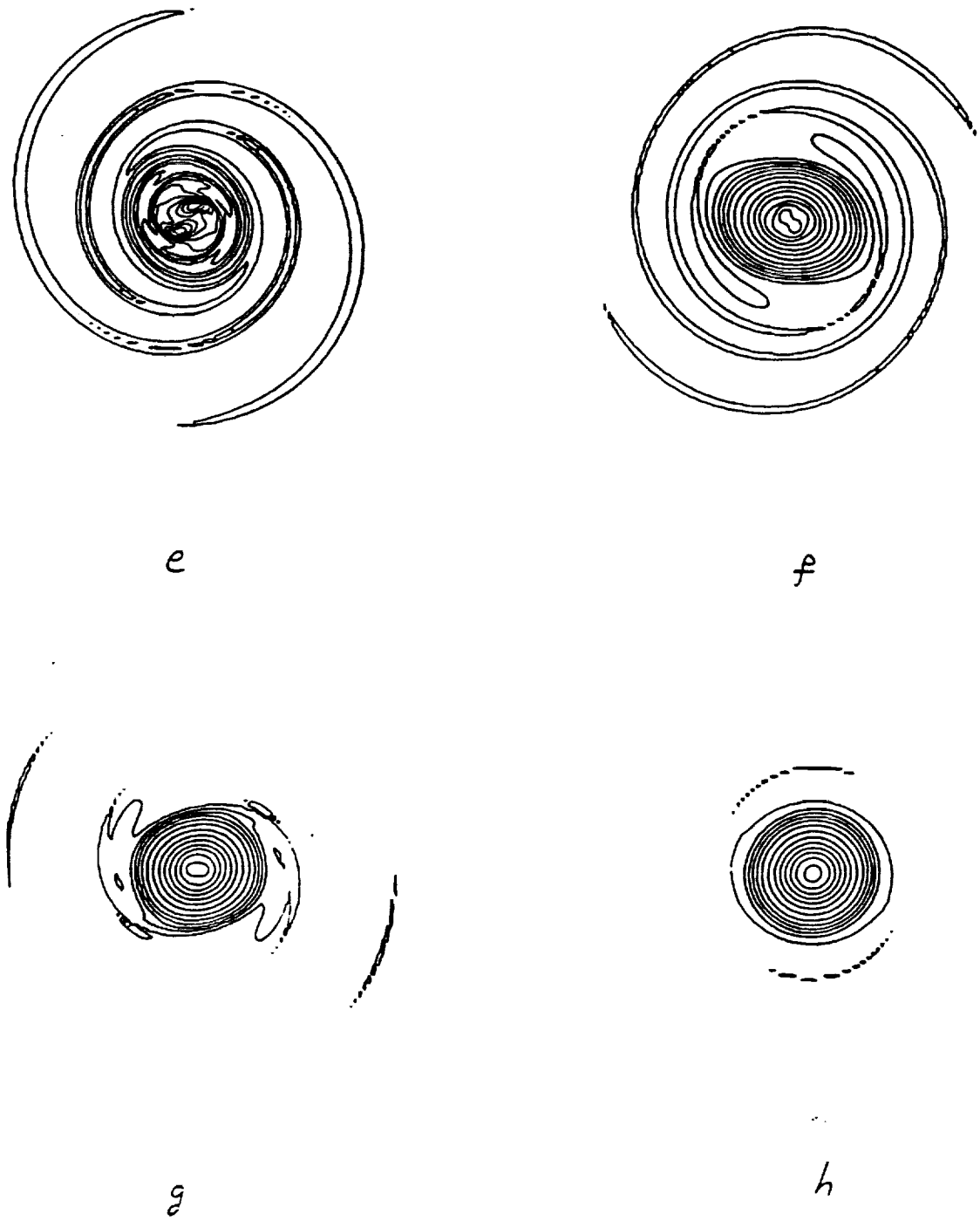

Fig. 11 The vorticity magnitude contours for the vortex pairing.

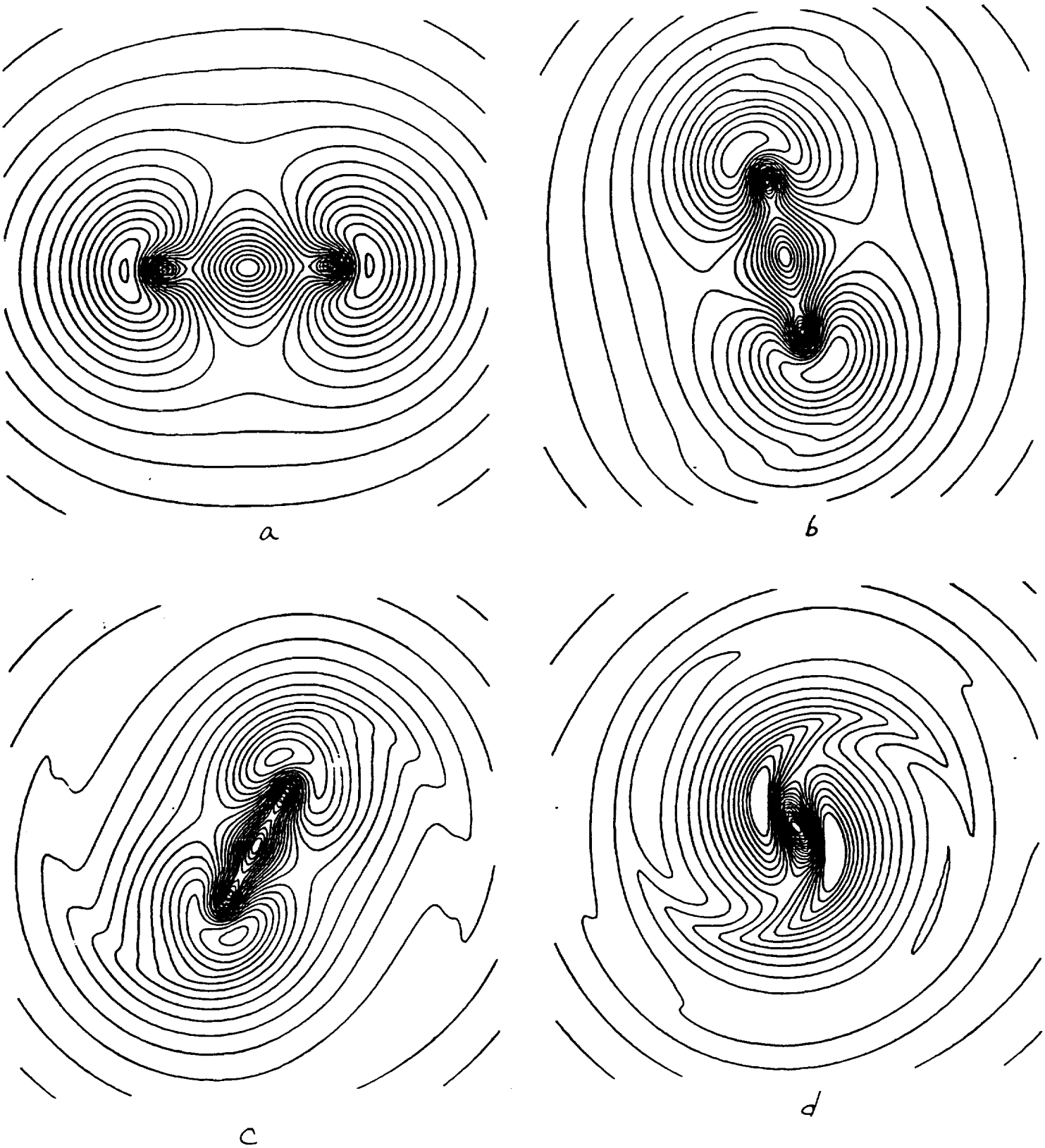

Fig. 12 The Mach number contours for the vortex pairing.

Appendix A

Organization - 1991

Position Chart

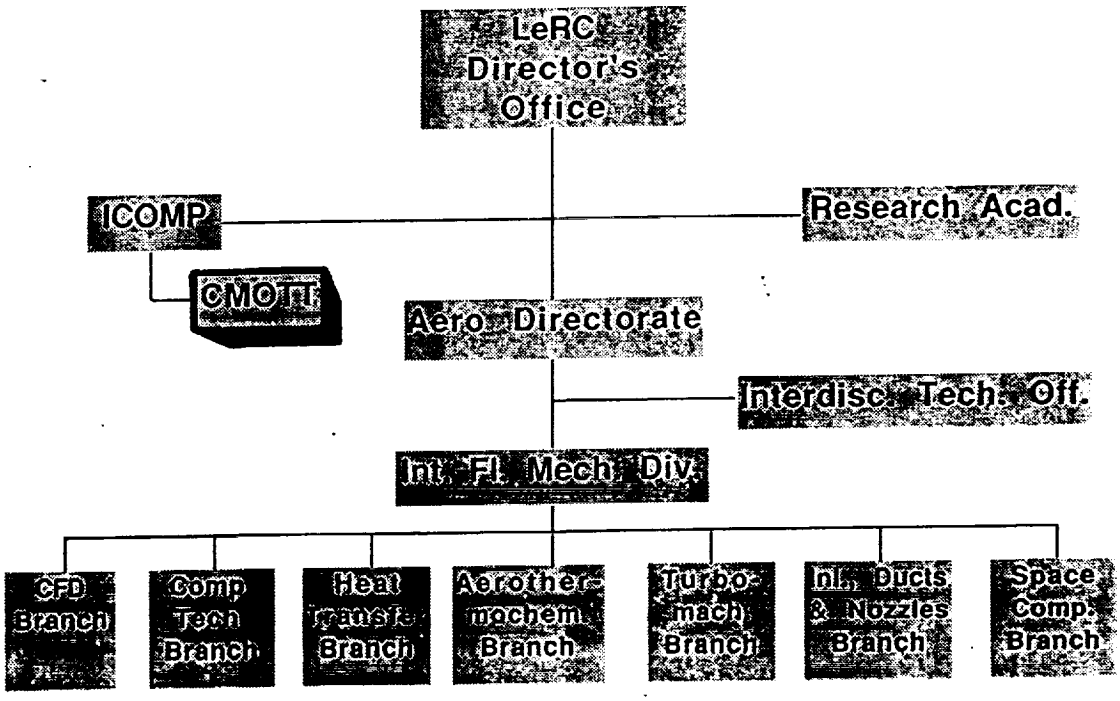

ICOMP Director

Dr. Louis A. Povinelli
Deputy Chief
Internal Fluid Mechanics Division
NASA Lewis Research Center

Coordinator

Dr. Meng-Sing Liou
Senior Scientist
Internal Fluid Mechanics Division
NASA Lewis Research Center

CMOTT Technical Leader

Dr. Tsan-Hsing Shih
Senior Research Associate
ICOMP, NASA Lewis Research Center

Advisors

Dr. Marvin E. Goldstein
Chief Scientist
NASA Lewis Research Center

Professor John L. Lumley
Sibley School of Mechanical and
Aerospace Engineering
Cornell University

Professor Eli Reshotko
Department of Mechanical and
Aerospace Engineering
Case Western Reserve University

Current Member Listing

Names/Term	Affiliation	Research Areas
Duncan, Beverly 7/1991 - present	Sverdrup Tech., Inc.	Multiple-Scale Turbulence Models
Hsu, Andrew T. 5/1990 - present	Sverdrup Tech., Inc.	PDF Turbulence Modeling, DNS
Liou, Meng-Sing 5/1990 - present	NASA LeRc	CFD Algorithms, High-Speed Flow
Liou, William W. 11/1990 - present	ICOMP	Compressible Flow Modeling, Weakly Nonlinear Wave Models
Rubinstein, Robert 7/1991 - present	Sverdrup Tech., Inc.	Analytical Theories of Turbulence
Shabbir, Aamir 5/1990 - present	ICOMP	Buoyancy Effects on Turbulence, Turbulence Modeling
Shih, Tsan-Hsing 5/1990 - present	ICOMP	Turbulence Modeling
Steffen, Christopher J. Jr. 10/1990 - present	NASA LeRc	Upwind Algorithms Incompressible Flow Two-Equation Turbulence Models
Van der Vegt, Jacobus J. 10/1991 - present	ICOMP	DNS Compressible Flows High Order Shock Capturing Schemes
Yang, Zhigang 7/1990 - present	ICOMP	Modeling of Bypass Transition
Yu, Sheng-Tao 3/1991 - present	Sverdrup Tech., Inc.	Modeling of Chemical Reacting Flows, DNS
Zhu, Jiang 4/1992 - present	ICOMP	Application of Turbulence Models in Complex Flows

Appendix B

CMOTT Biweekly Seminars / Technical Meetings

The purpose of these seminars is to exchange ideas and opinions on the latest developments and current state of turbulence and transition research. The speakers are invited from within and without of the NASA LeRC, including foreign speakers. The seminars were intended not noly to keep the members informed of the latest development of local turbulence and transition modeling research but also to increase interactions between group members and other researchers at the NASA LeRc.

The following is the meeting schedule and the abstract of the semainars during the reporting period.

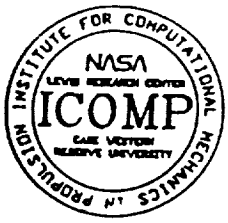

CENTER FOR MODELING OF TURBULENCE AND TRANSITION

Date: July 3, 1991

To: CMOTT Members and SVR and IFMD Staff

From: William W. Liou (6682)

Subject: CMOTT Biweekly Meeting

The following is a tentative schedule for the CMOTT biweekly get-together from July 10, 1991 to August 28, 1991.

The presentations will be informal and active participation is expected from the attendants. Soda and snack will be served in the meetings. These meetings complement the CMOTT Seminar Series, which are mainly formal presentations.

We would also appreciate some contributions from you. Subjects related to either the theoretical, experimental or computational aspects of turbulence and transition modeling are welcomed. Those who are willing to share their experience in these areas can contact me or Dr. T.-H. Shih at 6680 for further arrangement.

The meeting will start at 4:00 p.m. in Room 228, Sverdrup Building.

July 10, 1991	J. Lepicovsky (61-6753)	**LDV Measurement of Large Structures in a Tone Excited Turbulent Jet**
July 24, 1991	C. R. Wang (5865)	**Computations of Turbulence in a Shock/Turbulent Boundary Layer Interaction Flow**
August 7, 1991	A. Hsu (61-6648)	**PDF Turbulence Model and Its Applications**
August 28, 1991	C. Steffen (8508)	**DTNS: An Accurate and Efficient Testbed for Incompressible Flow Turbulence Modeling**

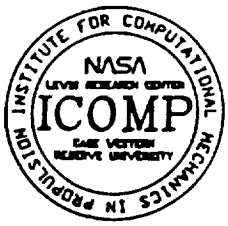

CENTER FOR MODELING OF TURBULENCE AND TRANSITION

Date: September 4, 1991

To: CMOTT Members and SVR and IFMD Staff

From: William W. Liou (6682)

Subject: CMOTT Biweekly Meeting

The following is a tentative schedule for the CMOTT biweekly get-together from **September 11, 1991** to **October 23, 1991** .

The presentations will be informal and active participation is expected from the attendants. Soda and snack will be served in the meetings. These meetings complement the CMOTT Seminar Series, which are mainly formal presentations.

We would also appreciate some contributions from you. Subjects related to either the theoretical, experimental or computational aspects of turbulence and transition modeling are welcomed. Those who are willing to share their experience in these areas can contact me or Dr. T.-H. Shih at 6680 for further arrangement.

The meeting will start at 4:00 p.m. in Room 228, Sverdrup Building.

Sept. 11, 1991 T. Bui (5639)
Implementation of the Chien Low-Re k-ϵ Models into the Proteus Code

Sept. 25, 1991 K. Ahn (5965)
A 2-D Oscillating Flow Analysis Using Quasi-steady Turbulence Model

October 9, 1991 J. Schwab (8446)
Variable-density Turbulence Modeling for Turbomachinery

October 23, 1991 M. Mawid (5965)
Multiphase Turbulent Combustion

CENTER FOR MODELING OF TURBULENCE AND TRANSITION

Date: November 4, 1991

To: CMOTT Members and SVR and IFMD Staff

From: William W. Liou (3-6682)

Subject: CMOTT Biweekly Meeting

The following is a tentative schedule for the CMOTT biweekly get-together from **November 6, 1991** to **December 18, 1991**.

This will be the last session of the CMOTT group-meetings/informal- seminars this year but the series will resume in mid-January 1992. Thank you for your patience and participation through out the year. The group-meetings/informal-seminars of CMOTT are meant not only to serve CMOTT members but also to provide an informal forum for those who are involved in transition/turbulence predictions. I thank all the speakers and participants who have made these objectives "realizable". Now, we are planing for 1992. If you have any suggestions or like to give a talk or two in the coming year, please call me or Dr. T. H. Shih at 3-6680. In the mean time, don't forget to mark your calendar for the following talks !

HAPPY HOLIDAYS !!!

The meeting will start at 4:00 p.m. in Room 228, Sverdrup Building.

Nov. 6, 1991 W. Liou (3-6682)
Weakly Nonlinear Models for Turbulent Free Shear Flows (2) - A Self-Contained Energy Transfer Model

Nov 20, 1991 D. Ashpis (3-8317)
DNS of Disturbances in Boundary Layer Flow

Dec. 4, 1991 B. Rubinstein (61-6612)
Analytical Theory of Turbulence and Turbulence Modeling: TSDIA and RNG

Dec. 18, 1991 B. Duncan (61-2998)
A New Three-Equation Model for Turbulence

CENTER FOR MODELING OF TURBULENCE AND TRANSITION

Date: January 30, 1992

To: CMOTT Members and SVR and IFMD Staff

From: William W. Liou (3-6682)

Subject: CMOTT Biweekly Meeting

The following is a tentative program for the CMOTT biweekly get-together/seminar from **February 5, 1992** to **March 18, 1992**. You are welcomed to join us.

Thanks to the your suggestions, we have made a few changes from last year's format. First, we have scheduled the CMOTT Seminar Series, which are mainly formal presentations, into the biweekly time frame of the CMOTT group-meeting/informal-talks. Also, the abstract of each presentation, formal or informal, will be distributed about one week prior to its scheduled date. Again, if you are interested in giving a presentation, please contact us.

The meeting will run from 1:30-2:15 PM in Room 145, Sverdrup Building, unless otherwise noted.

(1) Feb. 5, 1992 D. Davis
Weakly Nonlinear Vortex/Wave Interactions in Incompressible Cross-flow Boundary Layers in Transition

(2) Feb. 19, 1992 Z. Yang
A Modeling of Bypass Transition

(3) March 4, 1992 K. Zaman
Effect of "Delta-Tabs" on the Evolution of Axisymmetric Jets

(4) March 18, 1992 Professor R. M. C. So, Arizona State University
Near Wall Heat Transfer Modeling

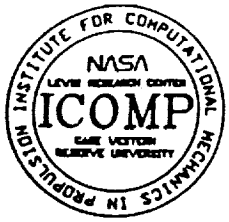

CENTER FOR MODELING OF TURBULENCE AND TRANSITION

Date: March 26, 1992

To: CMOTT Members and SVR and IFMD Staff

From: William W. Liou (3-6682)

Subject: CMOTT Biweekly Meeting

The following is a tentative program for the CMOTT biweekly get-together/seminar from **April 1, 1992** to **May 13, 1992**. You are welcomed to join us. Also, if you are interested in giving a presentation, please let us know.

The meeting will run from 1:30-2:15 PM in Room 228, Sverdrup Building, unless otherwise noted.

(5) April 1, 1992 J. Van der Vegt
The Development of an ENO-Osher Scheme for Direct Simulation of Compressible Flows

(6) April 15, 1992 J. Goodrich
Unsteady Time Asymptotic State: Incompressible Results, New Directions for Algorithms

(7) April 29, 1992 T.-H. Shih
Kolmogorov Behavior of Near-Wall Turbulence and Its Application in Turbulence Modeling

(8) May 13, 1992 Z. Yang
A Modeling of Bypass Transition

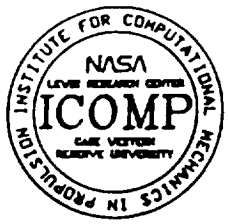

CENTER FOR MODELING OF TURBULENCE AND TRANSITION

Date: June 1, 1992

To: CMOTT Members and SVR and IFMD Staff

From: William W. Liou (3-6682)

Subject: CMOTT Biweekly Meeting

The following is a tentative program for the CMOTT biweekly get-together/seminar from **June 10, 1992** to **July 22, 1992**. You are welcomed to join us.

The talks will be informal and active participation will be expected from the audience.

Also, if you are interested in giving a presentation about the progress or some results of your own work on turbulence or transition, please let us know.

The meeting will run from 1:30-2:15 PM in Room 228, Sverdrup Building, unless otherwise noted.

(9) June 10, 1992 J. Zhu
Finite Volume Computations in Incompressible Flows with Complex Geometries

(10) June 24, 1992 J. Lee
RPLUS Code and Standard $k-\epsilon$ Models and Applications

(11) July 8, 1992 R. Mankbadi
Unsteady Turbulent Flows

(12) July 22, 1992 D. Rigby
The Effect of Spanwise Variations in Momentum on Leading Edge Heat Transfer

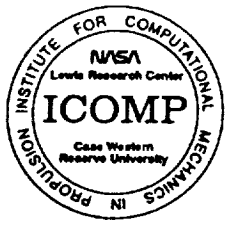

CENTER FOR MODELING OF TURBULENCE AND TRANSITION

Biweekly Meeting Series (1)

Weakly Nonlinear Vortex/Wave Interactions in Incompressible Crossflow Boundary Layers in Transition

by

Dominic Davis
ICOMP

Wed., 5 February, 1992
1:30-2:15 PM
Room 145, SVR Building

ABSTRACT

The instability of an incompressible three-dimensional boundary layer is considered theoretically and computationally in the context of vortex/wave interactions.Specifically the work centres on two low-amplitude, lower-branch Tollmien-Schlichting (TS) waves which mutually interact to induce a weak longitudinal vortex flow;the vortex motion,in turn,gives rise to significant wave-modulation via wall-shear forcing.The characteristic Reynolds number is taken as a large parameter and,as a consequence,the TS waves and the vortex are governed primarily by triple-deck theory.The nonlinear interaction is captured by a viscous partial-differential system for the vortex coupled with a pair of amplitude equations for the wave pressures. Computations were performed for relatively small crossflow values.Three distinct possibilities were found to emerge for the nonlinear behaviour of the flow solution downstream - an algebraic finite-distance singularity,far- downstream decay or repeated oscillations - depending on the various parameter values,the input amplitudes and the wave angles.

CENTER FOR MODELING OF TURBULENCE AND TRANSITION

Biweekly Meeting Series (1992-2)

A k-ϵ Model for Near Wall Turbulence and its Application in Turbulent Boundary Layer with/without Pressure Gradient

by

Z. Yang

ICOMP

Wed., 19 February, 1992
1:30-2:15 PM
Room 145, SVR Building

ABSTRACT

A $k-\epsilon$ model is proposed for turbulent wall bounded flows. In this model, turbulent velocity scale and turbulent time scale are used to define the eddy viscosity. The time scale used is bounded from below by the Kolmogorov time scale. The dissipation equation is reformulated using this time scale, removing the singularity of the high Reynolds number $k-\epsilon$ equation at the wall and rendering the introduction of the pseudo-dissipation unnecessary. The damping function used in the eddy viscosity is chosen to be a function of $R_y = \frac{k^{1/2}y}{\nu}$ instead of y^+. Thus, the model could be used for flows with separation. The model constants used are the same as the model constants in the commonly used high turbulent Reynolds standard $k-\epsilon$ model. Thus, the proposed model would reduce to the standard $k-\epsilon$ model when it is far away from the wall. Boundary layer flows at zero pressure gradient, favorable pressure gradient, adverse pressure gradient and increasingly adverse pressure gradient are calculated respectively. The comparisons of model predictions and the available experimental data are found to be good.

CENTER FOR MODELING OF TURBULENCE AND TRANSITION

Biweekly Meeting Series (1992-3)

Effect of Tabs on the Evolution of Axisymmetric Jets

by

Khairul Zaman

IFMD

Wed., 4 March, 1992
1:30-2:15 PM
Room 145, SVR Building

ABSTRACT

Vortex generators, in the form of small tabs at the nozzle exit, can have a profound influence on the evolution of an axisymmetric jet. Using tabs of certain shapes, the jet cross section can be distorted almost arbitrarily. Such distortion is accompanied by elimination of screech noise from supersonic jets and a significant increase in jet mixing. Key results obtained so far, covering a jet Mach number range of 0.3 and 1.8, will be summarized in this presentation. Observations will be made on the mechanisms of the effect including the likely vorticity dynamics in the flow.

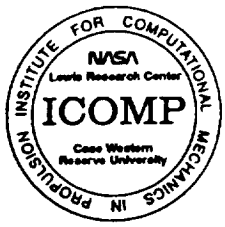

CENTER FOR MODELING OF TURBULENCE AND TRANSITION

Biweekly Meeting Series (1992-4)

Near-Wall Modeling of Turbulent Heat Transfer

by

Professor Ronald M. C. So

Mechanical and Aerospace Engineering
Arizona State University

Wed., 18 March, 1992
1:30-2:30 PM
Room 119, Building 5

ABSTRACT

A near-wall two-equation model for turbulent heat fluxes is derived from the temperature variance and its dissipation-rate equations and the assumption of gradient transport. The near-wall asymptotics of each term in the exact equations are examined and used to derive near-wall correction functions that render the modeled equations consistent with these behavior. Thus modeled, the equations are used to calculate fully-developed pipe and channel flows with hear transfer. It is found that the proposed two-equation model yields asymptotically correct near-wall behavior for the normal heat flux, the temperature variance and its near-wall budget and correct limiting wall values for these properties compared to direct simulation data and measurements obtained under different wall boundary conditions.

CONTACT: T.-H. Shih, PABX 3-5698

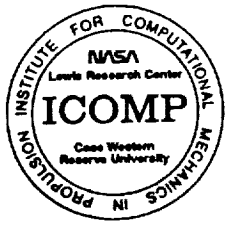

CENTER FOR MODELING OF TURBULENCE AND TRANSITION

Biweekly Meeting Series (1992-5)

The Development of an ENO-Osher Scheme for Direct Simulation of Compressible Flows

by

Jaap Van der Vegt

ICOMP

Wed., April 1, 1992
1:30-2:30 PM
Room 228, SVR Building

ABSTRACT

Direct simulation of turbulence and transition in compressible wall bounded flows presents an alternative to investigate important physical phenomena which are difficult to measure or study otherwise. It also provides data useful for turbulence modeling. A new program is being developed which solves the three-dimensional compressible Navier-Stokes equations using a higher order, fully implicit and time accurate ENO scheme together with Osher flux splitting. In this presentation an overview will be given of the numerical scheme and several test cases, both for supersonic and subsonic flow, will be presented and further improvements will be discussed.

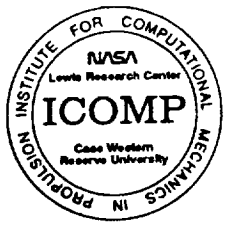

CENTER FOR MODELING OF TURBULENCE AND TRANSITION

Biweekly Meeting Series (1992-6)

Unsteady Time Asymptotic States: Incompressible Results and New Directions for Algorithms

by

John Goodrich

IFMD

Wed., April 15, 1992
1:30-2:15 PM
Room 228, SVR Building

ABSTRACT

Unsteady time asymptotic flow states for high Reynolds number viscous incompressible flow problems are presented. Discrete frequency flows are shown for the square driven cavity, with periodic cases for $Re = 9000$ and $Re = 9600$, and with aperiodic cases for $Re = 9700$ and $Re = 10000$. The algorithm for these calculations is based on the fourth order PDE for incompressible fluid flow which uses the streamfunction as the only dependent variable, it is second order accurate in space and time, and it has a stability constraint of $CFL \leq 1$. The algorithm is extremely robust with respect to Reynolds number.

The direct numerical simulation of transition and turbulence requires numerical methods to be more than second order accurate in order to accurately represent the relevant scales of the physical processes. Recently developed finite difference algorithms are presented for unsteady convection equations, including the advection and inviscid Burgers equation in one space dimension, and the wave equation treated as a system, with remarks on diffusion equations and extension to higher space dimensions. The new algorithms that will be discussed all use local stencils, they range from third to seventh order in accuracy, they all have the same order of accuracy in both space and time, and they are all one step explicit methods (except for diffusion equations). Since all of the algorithms use a small local stencil, the number of degrees of freedom of known data required for higher order accuracy is obtained by higher information density than just the solution data. The use of a two point stencil (for some of the methods) allows for arbitrary grid spacing, though a convective stability constraint must be observed at each grid point. The use of local data for an explicit algorithm with high order accuracy avoids the requirement of using a global solution method such as compact differencing or spline based algorithms. There will be computational results for all of the algorithms that are presented.

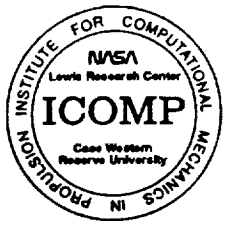

CENTER FOR MODELING OF TURBULENCE AND TRANSITION

Biweekly Meeting Series (1992-7)

Kolmogorov Behavior of Near-Wall Turbulence and Its Application in Turbulence Modeling

by

Tsan-Hsing Shih

ICOMP

Wed., April 29, 1992
1:30-2:15 PM
Room 228, SVR Building

ABSTRACT

The near-wall behavior of turbulence is re-examined in a way different from that proposed by Hanjalic and Launder[1] and followers[2],[3],[4],[5]. It is shown that at a certain distance from the wall, all energetic large eddies will reduce to *Kolmogorov* eddies (the smallest eddies in turbulence). All the important wall parameters, such as friction velocity, viscous length scale, and mean strain rate at the wall, are characterized by *Kolmogorov* microscales. According to this *Kolmogorov* behavior of near-wall turbulence, the turbulence quantities, such as turbulent kinetic energy, dissipation rate, etc. at the location where the large eddies become "*Kolmogorov*" eddies, can be estimated by using both direct numerical simulation (DNS) data and asymptotic analysis of near-wall turbulence. This information will provide useful boundary conditions for the turbulent transport equations. As an example, the concept is incorporated in the standard k-ϵ model which is then applied to channel and boundary layer flows. Using appropriate boundary conditions (based on *Kolmogorov* behavior of near-wall turbulence), there is no need for any wall-modification to the k-ϵ equations (including model constants). Results compare very well with the DNS and experimental data.

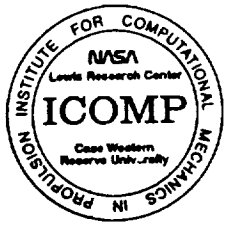

CENTER FOR MODELING OF TURBULENCE AND TRANSITION

Biweekly Meeting Series (1992-8)

A Modeling of Bypass Transition

by

Z. Yang

ICOMP

Wed., May 13, 1992
1:30-2:15 PM
Room 228, SVR Building

ABSTRACT

A model for the calculation of bypass transitional boundary layers due to the freestream turbulence is proposed. The model combines a near wall $k-\epsilon$ model proposed for the fully developed turbulent flows with the intermittency of the transitional boundary layers. The intermittency factor is assumed to be a function of both the free stream turbulence and the shape factor of the boundary layer. Transitional boundary layers over a flat plate with different freestream turbulence level are calculated using the proposed model. It is found that the model calculations agree well with the experimental data and give a better prediction compared with other low Reynolds number $k-\epsilon$ models, which do not incorporate the intermittency effect.

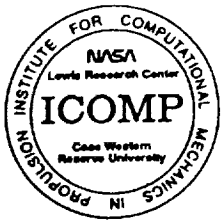

CENTER FOR MODELING OF TURBULENCE AND TRANSITION

Biweekly Meeting Series (1992-9)

Finite-Volume Computations of Incompressible Flows with Complex Geometries

by

J. Zhu

ICOMP

Wed., June 10, 1992
1:30-2:30 PM
Room 228, SVR Building

ABSTRACT

A brief review is given of finite-volume procedures developed at the Institute for Hydromechanics, University of Karlsruhe, for calculating incompressible elliptic flows with complex boundaries. The procedures include: numerical grid generation, higher-order bounded convection schemes, zonal solution, simulation of two-phase flows, and near-wall turbulence modelling. Various application examples will be given.

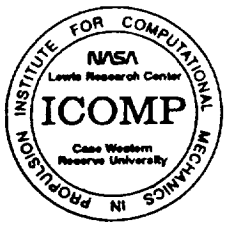

CENTER FOR MODELING OF TURBULENCE AND TRANSITION

Biweekly Meeting Series (1992-10)

Development of the RPLUS code with Standard $k-\epsilon$ model and Their Applications

by

Jinho Lee
Sverdrup Technology, Inc.

Wed., June 24, 1992
1:30-2:30 PM
Room 228, SVR Building

ABSTRACT

The primary goal of this research effort is to develop a CFD tool which can be used in a variety of practical supersonic/hypersonic propulsion device development/analysis environments. One focus of this work has been to develop and validate the Reactive Propulsion code based on LU Scheme(RPLUS). This effort also includes the development of turbulence models which can be used in the predictions of highly complex flow environments inside of combustors.

This presentation will cover only a small part of a larger development effort and focus will primarily on the analysis, implementation, and development of the turbulence model capabilities of the RPLUS code.

Some of the issues which will be covered are; formulation of the turbulence models, the numerical technique used to solve the turbulence model equations, and modeling of compressibility effects. The primary numerical technique used in the RPLUS code is the LU-SSOR(LU scheme based on Successive Symmetric Over Relaxation) technique. Therefore, the turbulent kinetic energy transport and dissipation transport equations are also solved using the LU-SSOR numerical technique.

Both two and three dimensional turbulence model development are being developed for the RPLUS code. However, the majority of the presentation will focus on the development of the two dimensional k-ϵ models for the RPLUS code. Issues regarding compressible wall-function boundary conditions and compressibility effects will be addressed. Both low and high Reynolds number forms of the k-ϵ models are being developed. The "standard" low Reynolds number model of Launder-Sharma and Chien has been used in this study. The problems of primary interests are supersonic turbulent boundary-layers, shock-wave/boundary-layer interactions, and shear-layers in two or three dimensional environments.

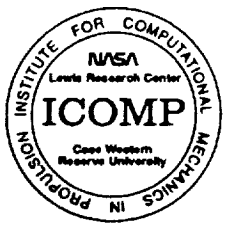

CENTER FOR MODELING OF TURBULENCE AND TRANSITION

Biweekly Meeting Series (1992-11)

Unsteady Turbulent Flows

by

Reda R. Mankbadi
NASA Lewis Research Center

Wed., July 8, 1992
1:30-2:30 PM
Room 228, SVR Building

ABSTRACT

Current research activities emphasize computation/modelling of turbulent flows when basic flow is time-periodic. Wall-bounded flows and free shear flows exhibit different features when the basic flow is unsteady; and as such, different approaches are used to model them.

(A) In wall-bounded, oscillatory flows, two approaches are used to model turbulence: (I) Turbulence is assumed to behave in a quasi-steady manner, and steady-state models are directly extended to the unsteady case. This approach fails at high frequencies of oscillations. (II) Rapid distortion theory (RDT) is successfully adapted to aid in turbulence modelling of highly unsteady flows (high frequencies). The eddy viscosity hypothesis is replaced by the ratio of turbulent stresses/kinetic energy; which is given by RDT as a function of the accumulated rate of strain.

(B) In free shear flows (naturally unsteady, or excited to be unsteady), two approaches are investigated: (I) The large-scale (organized, coherent) component is modelled as instability waves interacting with each other as well as with the mean flow and the fine-scale (random, background) turbulence. Integrated kinetic-energy equations are then obtained for each scale of motion. The approach is successful in predicting results in good agreements with experiments in which excitation devices are used to control jet mixing and turbulence. (II) The other approach adopted is Large-Eddy Simulations (LES) with application to predicting the far-field noise of a supersonic jet.

CONTACT: William W. Liou, PABX 3-6682

C-3

CENTER FOR MODELING OF TURBULENCE AND TRANSITION

Biweekly Meeting Series (1992-12)

The Effect of Spanwise Variations in Momentum on Leading Edge Heat Transfer

by

David Rigby
Sverdrup Tech. INc.

Wed., July 22, 1992
1:30-2:30 PM
Room 228, SVR Building

ABSTRACT

A study of the effect of spanwise variation in momentum on leading edge heat transfer is discussed. Numerical and experimental results are presented for a circular leading edge and for a 3:1 elliptical leading edge. Direct comparison of the two-dimensional results, that is with no spanwise variations, to the analytical results of Frossling is very good. The numerical calculation, using the PARC3D code, solves the three-dimensional Navier-Stokes equations, assuming steady laminar flow on the leading edge region. Experimentally, increases in spanwise averaged heat transfer coefficient as high as 50% above the two-dimensional value were observed. Numerically, the heat transfer coefficient was seen to increase by as much as 25% percent. In general, the circular leading edge, under the same flow conditions, produced a higher heat transfer rate than the elliptical leading edge. As a percentage of the respective two-dimensional values, the circular and elliptical leading edges showed similar sensitivity to spanwise variations in momentum. By equating the root mean square of the amplitude of the spanwise variation in momentum to the turbulence intensity, a qualitative comparison between the present work and turbulent results was possible.

CONTACT: William W. Liou, PABX 3-6682

Appendix C
List of Member's Publications

Barton, J. M., Rubinstein, R. and Kirtley, K. R. "Nonlinear Reynolds Stress Model for Turbulent Shear Flows, " AIAA Paper No. 91-0609, (Jan. 1991).

Barton, J. M. and Rubinstein, R., "Nonlinerar Algebraic Reynolds Stress Model for Anisotropic Turbulent Flows, " 11th U. S. National Congress of Applied Mechanics, Tucson, AZ (May 1990).

Barton, J. M. and Rubinstein, R., "Renormalization Group Theory and Turbulence Modeling, " 2nd International Workshop on Chaos and Turbulence, Tsukuba, Japan (Jan. 1992).

Barton, J. M. and Rubinstein, R., "Renormalization Group Analysis of Turbulence-Driven Secondary Fows, " 11th Australian Fluid Mechanics Conference, Hobart, Australia (Dec. 1992).

Brown, S., Leibovich, S. and Z. Yang, "On the linear instability of the Hall-Stewartson vortex," Theoretical and Computational Fluid Dynamics, **2**, 27-46, (1990).

Duncan, B. S., Liou, W. W. and Shih, T.-H., "A Multiple-scale turbulence model for incompressible flow," NASA TM (to appear) (1992).

Duncan, B.S., Lumley, J.L., Shih, T.H. and To, W.M., "A new model for the turbulent dissipation" International Conference of Fluid Mechanics and Theoretical Physics, Bejing, China (1992).

Hsu, A.T. and Liou, M., "Computational analysis of underexpanded jets in the hypersonic regime," Journal of Propulsion and Power, **7**, No. 2, (1991).

Hsu, A.T., "Progress in the development of PDF turbulence models for combustion," 10th NASP Symposium, April 23-16, 1991, Monterey, California.

Hsu, A.T., "A study of hydrogen diffusion flames using PDF turbulence model," AIAA 91-1780, AIAA 22nd Fluid Dynamics Conference, June 24-26, 1991, Honolulu, Hawaii.

Hsu, A.T. and Chen, J.Y., "A continuous mixing Model for PDF simulations and its applications to combusting shear flows," 8th International Symposium on Turbulence Shear Flows, Sept. 9-11, 1991, Munich, Germany.

Lang, N.J. and Shih, T.-H., "A critical comparison of two-equation turbulence models," NASA TM 105237, (1991).

Liou, M. S. and Steffen, Jr., C. J., "A New Flux Splitting Scheme," NASA TM 104404 (1991).

Liou, W. W. and Shih, T.-H., "A two-scale model for compressible turbulent flows," NASA TM (to appear) (1992).

Liou, W. W. and Shih, T.-H., "On the basic equations for sencond-order modeling of compressible turbulence," NASA TM 105277 (1991).

Liou, W. W. and Morris, P. J., "Weakly nonlinear models for turbulent mixing in a plane mixing layer," Phy. Fluids (to appear).

Liou, W. W. and Morris, P. J., "The eigenvalue specturm of the Rayleigh equation for a plane shear layer," Int. J. Num. Fluids, (to appear).

Liou, W. W., "A new energy transfer model for turbulent free shear flow," NASA TM (to appear) (1992).

Mansour, N N. and Shih, T.-H. and Reynolds, W. C., "The effects of rotation on initially anisotropic homogeneous flows," Physics of fluid A, **3**, 10, 2421-2425 (1991).

Michelassi, V. and Shih, T.-H., "Low Reynolds number two-equation modeling of turbulent flows," NASA TM 104368, (1991).

Michelassi, V. and Shih, T.-H., "Elliptic flow computation by low Reynolds number two-equation turbulence models ," NASA TM 105376, (1991).

Moin, P., Shih, T.-H., Driver, D. and Mansour, N., "Direct numerical simulation of a three-dimensional turbulent boundary layer," Physics of Fluids A **2**, 10, 1846-1853 (1990).

Rubinstein, R. and Barton, J. M., "Nonlinear Reynolds stress models and the renormalization group," Phys. Fluids A **2**, 1472 (1990).

Rubinstein, R. and Barton, J. M., "Renormalization group analysis of anisotropic diffusion in turbulent shear flow," Phys. Fluids A **3**, 415 (1991).

Rubinstein, R. and Barton, J. M., "Renormalization group analysis of the Reynolds stress transport equation," to appear in Physics of Fluids A, (July 1992).

Shabbir, Munich. A., "Experimental balances for the second moments for a buoyant plume and their implication on turbulence modeling," Eighth Symposium on Turbulent Shear Flows, 27-1-1 to 27-1-6 (1991).

Shabbir, A. and Shih, T.-H., "Critical comparison of second order turbulence models in homogeneous flows," Submitted to AIAA Annual meeting in Reno, Jan. 1992.

Shih, T.-H. and Lumley, J.L., "Kolmogorov behavior of near-wall turbulence and its application in turbulence modeling," NASA TM 105663 (1992)

Shih, T.-H., Chen, J.-Y. and Lumley, J. L., "Second order modeling of free turbulent shear flows," AIAA Journal, **30**, 6, 1553-1560 (1992).

Shih, T.-H. and Lumley, J.L., "A critical comparison of second order closures with direct numerical simulation of homogeneous turbulence," NASA TM 105351 (1991).

Shih, T.-H. and Hsu, A.-T., "An improved $k - \epsilon$ model for near-wall turbulence," AIAA paper, 91-0611 (1991).

Shih, T.-H. Shih, Shabbir, A. and Lumley, J.L., "Advances in Modeling the pressure correlation terms in the second moment equations," *The Lumley Symposium: Resent Developments in Turbulence*, November, 12-13, 1990, ICASE, NASA Langley Research Center, Edited by Gatski, T.B., Sarkar, S., Speziale, C.G.

Shih, T.-H., "An improved $k - \epsilon$ model for near-wall turbulence and comparison with direct numerical simulation," NASA TM 103221 (1990).

Shih, T.-H. and Mansour, N. N., "Modeling of near-wall turbulence," *Engineering Turbulence Modeling and Experiments*, September 24-28, 1990, Dubrovnik, Yugoslavia, Editors: W.Rodi, E.N. Ganic.

Shih, T.-H. and Reynolds, W. C., "A spectrum model for weakly anisotropic turbulence," Physics of Fluids A, **2**, 8, (1990).

Steffen, Jr., C. J., "An Investigation of DTNS2D for Use as an Incompressible Turbulence Modelling Test-Bed," NASA TM 105593 (1992).

Steffen, Jr., C. J. and Beard, L. M., "Incompressible Navier Stokes Solutions Using the Pseudo Compressibility Technique," *Proceeding of the 23rd Annual Pittsburgh Conference on Modeling and Simulation*, in print (1992).

Van der Vegt, Jaap, "ENO-Osher schems for Euler equations," submitted for publication (1992).

Van der Vegt, Jaap, "Overview of the Osher approximate Riemann solver for three-dimensional flows," NASA TM, in print (1992).

Yang, Z. and Leibovich, S "Nonlinear dynamics near the stability margin in rotating pipe flow," J. Fluid Mech. **233**, 329-347, (1991).

Yang, Z. and Leibovich, S., "Unstable viscous wall modes in rotating pipe flow," AIAA Paper 91-1801, (1991). Also submitted to Physics Fluids A for publication.

Yang, Z. and Shih, T.H., "A $k - \epsilon$ modeling of near wall turbulence," Proc. of 4th Intl. Sym. on CFD, Davis, CA, 1305-1310, (1991). Also available as NASA TM 105238.

Yang, Z. and Shih, T.H., "A $k-\epsilon$ calculation of transitional boundary layers," To appear in *Transition and Turbulence*, Springer-Verlag, 1992. Also available as NASA TM 105604.

Yang, Z. and Shih, T.H. "A new time scale based $k-\epsilon$ model for near wall turbulence," Submitted for publication. It is also to appear as a NASA TM (1992).

Yang, Z. and Shih, T. H., "A modeling of transitional boundary layers," In preparation.

Zhu, G., Lai, M.-C and Shih, T.-H., "Second-order closure modeling of turbulent buoyant wall plumes," NASA TM (in print) (1992).

REPORT DOCUMENTATION PAGE

Form Approved
OMB No. 0704-0188

1. AGENCY USE ONLY (*Leave blank*)	2. REPORT DATE	3. REPORT TYPE AND DATES COVERED
	September 1992	Technical Memorandum

4. TITLE AND SUBTITLE

Center for Modeling of Turbulence and Transition (CMOTT)

Research Briefs–1992

5. FUNDING NUMBERS

WU–505–62–21

6. AUTHOR(S)

7. PERFORMING ORGANIZATION NAME(S) AND ADDRESS(ES)

National Aeronautics and Space Administration
Lewis Research Center
Cleveland, Ohio 44135–3191

8. PERFORMING ORGANIZATION REPORT NUMBER

E–7274

9. SPONSORING/MONITORING AGENCY NAMES(S) AND ADDRESS(ES)

National Aeronautics and Space Administration
Washington, D.C. 20546–0001

10. SPONSORING/MONITORING AGENCY REPORT NUMBER

NASA TM–105834
ICOMP–92–12; CMOTT–92–08

11. SUPPLEMENTARY NOTES

Report compiled by William W. Liou and T.-H. Shih, NASA Lewis Research Center (work funded under NASA Cooperative Agreement NCC3–233). ICOMP Program Director: Louis A. Povinelli, (216) 433–5818.

12a. DISTRIBUTION/AVAILABILITY STATEMENT

Unclassified - Unlimited
Subject Category 34

12b. DISTRIBUTION CODE

13. ABSTRACT (*Maximum 200 words*)

This research brief contains the progress reports of the Research Staff of the Center for Modeling of Turbulence and Transition (CMOTT) from May 1991 to May 1992. It is intended as an annual report to the Institute for Computational Mechanics in Propulsion and NASA Lewis Research Center. A separate report entitled, "Workshop on Engineering Turbulence Modeling," covering some of the 1991 CMOTT Summer research activities was released earlier this year. The main objective of the CMOTT is to develop, validate and implement the turbulence and transition models for practical engineering flows. The flows of interest are three-dimensional, incompressible and compressible flows with chemical reaction. During this period, the research covers two-equation (e.g., k-ε) and algebraic Reynolds-stress models, second moment closure models, probability density function (pdf) models, Renormalization Group Theory (RNG), Large Eddy Simulation (LES) and Direct Numerical Simulation (DNS). Last year was CMOTT's second year in operation. CMOTT now has eleven members from ICOMP, NASA LeRC, and Sverdrup Technology Inc., working on various aspects of turbulence and transition modeling in collaboration with NASA-Lewis scientists and Case Western Reserve University faculty members. The CMOTT members have been continuously and actively involved in the international and national turbulence research activities. A biweekly CMOTT seminar series has been conducted with speakers invited from within and without the NASA Lewis Research Center, including foreign speakers. The current CMOTT roster and its organization are listed in Appendix A. Listed in Appendix B are the abstracts and the scientific and technical issues discussed in biweekly CMOTT seminars. Appendix C gives a list of references which are the papers contributed by CMOTT members in the last two years.

14. SUBJECT TERMS

Turbulence models

15. NUMBER OF PAGES

192

16. PRICE CODE

A09

17. SECURITY CLASSIFICATION OF REPORT	18. SECURITY CLASSIFICATION OF THIS PAGE	19. SECURITY CLASSIFICATION OF ABSTRACT	20. LIMITATION OF ABSTRACT
Unclassified	Unclassified	Unclassified	